Available online at www.sciencedirect.com

ScienceDirect

Underground Space 26 (2026) 435–457

www.keaipublishing.com/undsp

Research Paper

Carbon emission mechanism and influence of design-oriented railway tunnel engineering

Yajuan Li, Xueying Bao *

School of Civil Engineering, Lanzhou Jiaotong University, Lanzhou 730070, China

Received 13 April 2025; received in revised form 14 September 2025; accepted 26 September 2025
Available online 4 December 2025

Abstract

Tunnels are critical transportation infrastructure, with >80% of their lifecycle carbon emissions from the design phase. Therefore, low-carbon design is a pathway to achieving "zero carbon" goals. However, multi-source and heterogeneous design information creates challenges because of tunnel carbon emission data silos. This study proposes a carbon emissions-structure-design framework with a multi-layered integrated structure for tunnel carbon footprint assessment, clarifying the relationships among design parameters, structural characteristics, and carbon emissions. Additionally, a design structure matrix-carbon footprint model is established to analyze the relationships between low-carbon design elements (LDEs) and the lifecycle carbon footprint. A model is developed to examine the nonlinear mechanisms by which LDEs affect carbon emissions. Case studies indicate that carbon emissions during the construction phase primarily arise from tunnel boring machine excavation, slag transportation, shotcreting, and tunnel lining. They are significantly influenced by LDEs, such as the surrounding rock grade, tunnel radius, advance rate, and slope, which exhibit threshold effects. In the operational phase, carbon emissions are dominated by train traction energy consumption, which increases with speed and decreases with radius. This is in contrast to the construction phase, where larger radii lead to higher emissions. This study integrates tunnel design parameters with lifecycle carbon emissions to overcome the limitations of traditional segmented approaches. The findings provide a decision-support framework for source-level emission reduction during the design phase, enabling engineers to predict carbon emissions for parameter combinations and offer a new strategy for achieving carbon neutrality in transportation infrastructure.

Keywords: Low-carbon design elements; Carbon emissions-structure-design framework; Design structure matrix-carbon footprint model; Lifecycle carbon emissions; Nonlinear mechanisms

1 Introduction

Compared to conventional transportation infrastructure, tunnels are considered to exhibit higher energy, material, and carbon emission densities (Guo et al., 2016), resulting in a considerable environmental burden. The semi-enclosed geometry of tunnels leads to CO_2 concentrations that are three to five times higher than ambient levels. When the CO_2 concentration increases from 400×10^6 to 800×10^6, the carbonation depth of the concrete increases by 1.41 times (Denning, 2018), substantially increasing the risk of durability failure (Bastidas-Arteaga et al., 2013) and potentially compromising tunnel operational safety (Lee & Ellingwood, 2017). Therefore, it is imperative to reduce carbon emissions throughout the lifecycle of tunnel engineering.

Tunnel engineering design significantly influences lifecycle CO_2 emissions, contributing up to 80% of the total emissions (Kanyilmaz et al., 2023). The integration of low-carbon principles during early design stages is critical for reducing emissions at the source. These emissions are influenced by several factors. As demonstrated by Spyridis and Bergmeister (2024), design assumptions and decisions regarding material properties, structural characteristics,

* Corresponding author.
E-mail address: baoxueying@lzjtu.edu.cn (X. Bao).
Peer review under the responsibility of Tongji University

https://doi.org/10.1016/j.undsp.2025.09.004

and their applications can substantially reduce material consumption through optimized design solutions, thereby lowering carbon emissions during both the construction and operation phases. Therefore, a low-carbon design approach has proven to be an effective strategy for minimizing emissions at the source.

Research on carbon emissions in tunnel engineering has evolved from assessments focusing solely on the construction phase to comprehensive lifecycle analyses. Early studies primarily quantified the emissions during construction. For example, Zhao et al. (2022) reported carbon emissions of 60 296 kg per ring for slurry shield tunnels, whereas Liu et al. (2024) found that the embedded carbon per unit length increased exponentially with the deterioration of the surrounding rock, ranging from 7.97 to 24.27 t. Y. Guo et al. (2025) estimated the total emissions during construction to be 627 807.38 t. As assessment dimensions expanded, Song et al. (2024a) revealed that on-site construction emissions reached 2.643×10^7 kg CO_2e, with annual operation and maintenance emissions amounting to 7.765×10^4 kg CO_2e. Although significant progress has been made in quantifying tunnel carbon emissions, understanding the underlying driving mechanisms remains essential for developing reduction strategies. Recent studies focused on elucidating these complexities. Xu et al. (2021) identified the driving factors in lining construction, and Rodríguez et al. (2020, 2024) developed a multi-parameter assessment model for carbon emissions. In addition, Chen et al. (2024, 2025) established models that link geotechnical parameters, tunnel boring machine (TBM) efficiency, and carbon emissions, thereby contributing substantially to the tunnel engineering field. Insights from other disciplines, where studies have analyzed the influence of various factors on carbon emissions (Wang & Ma, 2024; Ma et al., 2025; Wang et al., 2025), also offer valuable perspectives for tunnel engineering.

Although research on the mechanisms influencing carbon emissions in tunnel engineering has advanced, a systematic analysis of the dynamic relationship between lifecycle design variables and carbon emissions remains lacking. As the starting point of the tunnel lifecycle, plans developed during the design phase exert chain-like effects on carbon emission characteristics throughout construction and operation via technical path-transmission mechanisms. However, the transmission paths, effect intensities, and evolutionary patterns of these inter-phase impacts are poorly understood. This results in a "black box" regarding how design variables influence lifecycle carbon emissions, which constrains systematic decision-making support for the low-carbon transformation of engineering projects.

Therefore, this study focuses on railway tunnels and investigates the impact mechanisms through which low-carbon design elements (LDEs) influence carbon emissions throughout the tunnel lifecycle. It aims to transcend the traditional experience-driven design paradigm by adopting a carbon-flow-driven low-carbon design methodology, thereby facilitating significant emission reductions at the source. To achieve this, an innovative carbon emissions-structure-design (C-S-D) model is proposed to establish a multi-layer integrated framework for tunnel carbon emissions. Subsequently, a design structure matrix-carbon footprint (DSM-CF) model is developed to analyze the relationship between LDEs and carbon emissions during the construction and operation phases. Finally, a quantitative model is introduced to reveal the nonlinear mechanisms of LDEs within the lifecycle carbon flow. The research findings provide tunnel designers with a decision-making tool for quantifying carbon emissions and theoretical support for optimizing low-carbon design strategies. Additionally, they present a practical pathway for transitioning carbon reduction in tunnel engineering from a single-stage quantification approach to a full lifecycle management paradigm. These contributions hold substantial practical significance for achieving low-carbon transformation in the tunnel engineering industry.

2 Integrated framework for tunnel engineering carbon footprint assessment

As a fundamental component of railway tunnel engineering design, the structure itself does not directly produce carbon emissions; however, its construction and operational use can lead to significant emissions influenced by the design. This study establishes a C-S-D model to clarify the relationship between tunnel engineering design and the carbon footprint across the construction and operation stages. This model considers LDEs as inputs and the carbon footprints from construction and operational activities as outputs, creating a multi-level framework to analyze how tunnel design affects lifecycle carbon emissions (Peng et al., 2019; Kong et al., 2021).

The framework consists of five layers: engineering, structure, design elements, construction process, and operation. The engineering layer refers to tunnel engineering. The structure (S) layer serves as the foundation for realizing tunnel engineering functions, including tunnel support, tunnel lining, waterproofing, and drainage. The design element (DE) layer comprises a series of LDEs, which are core components that influence carbon emissions during the construction and operation stages and are essential for low-carbon tunnel design (Jun et al., 2019). The construction process (CP) layer encompasses the activities required to realize the structural design, including tunnel excavation, slag transportation, and shotcrete. The operation (O) layer encompasses the application processes of the structural entity, including ventilation and lighting operation, as illustrated in Fig. 1.

The S and DE layers represent the design domain, whereas the CP and O layers represent the emission domain. There are one-to-one, one-to-many, many-to-one, and many-to-many relationships between the design and carbon emission domains. The set of factors in the design domain is denoted as set X, whereas the set of fac-

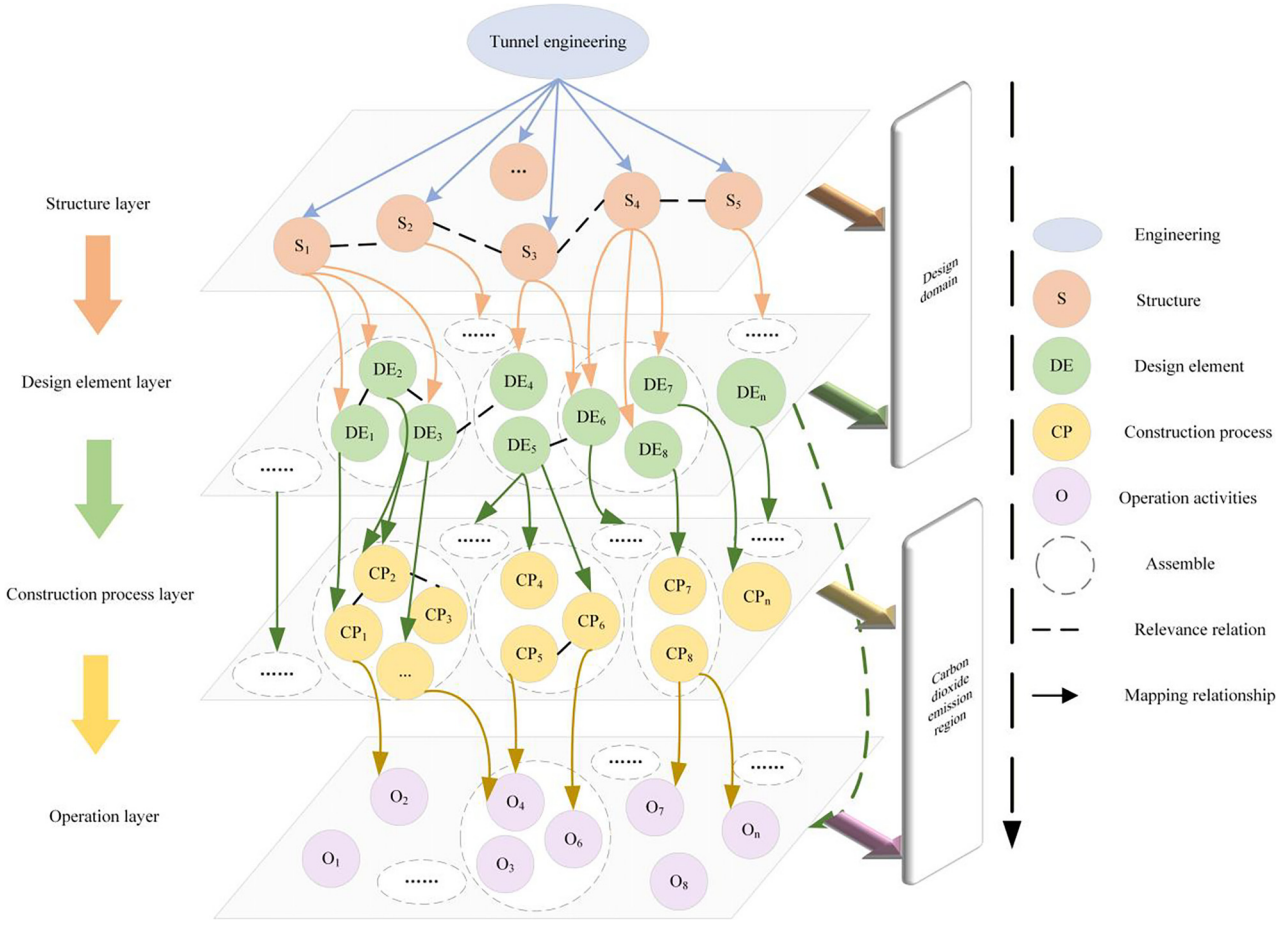

Fig. 1. Multi-layer integrated framework for tunnel engineering carbon footprint assessment.

tors in the carbon emission domain is denoted as set Y. Therefore, the correlation function $f(x)$ between the design and carbon emission domains can be expressed as follows:
One-to-one relationship: $X \rightarrow Y: y = f_1(x)$,
One-to-many relationship: $X \rightarrow Y: (y_1, y_2, \cdots, y_n) = f_2(x)$,
Many-to-one relationship: $X \rightarrow Y: y = f_3(x_1, x_2, \cdots, x_m)$,
Many-to-many relationship: $X \rightarrow Y: (y_1, y_2, \cdots, y_n) = f_4(x_1, x_2, \cdots, x_m)$.

3 Determination of tunnel engineering carbon emission boundaries

This study defines the carbon emission boundaries from three perspectives: gaseous, engineering, and temporal.

Gaseous boundary: CO_2 accounts for approximately 63% of the total warming effect of greenhouse gases (GHGs) (IStructE, 2022) and plays a significant role in global warming. As international emission reduction policies primarily target CO_2, this study focuses exclusively on CO_2 emissions; other GHGs are excluded.

Engineering boundary: Tunnel engineering is divided into tunnel excavation, support, lining, waterproofing and drainage, ventilation, and lighting. As railway tunnels frequently traverse hard rock, the drill-and-blast and TBM are the main construction methods. The shield tunneling method, which is suited for soft soil and water-bearing strata, is not considered in this study. Research has shown that the drill-and-blast method produces stable carbon emissions of 1500 to 2000 kg CO_2e/km (G. Guo et al., 2025), which limits its potential for further reduction. In contrast, the TBM method relies on electric or diesel power, resulting in higher variability in emissions, ranging from 8000 to 16 000 kg CO_2e/km (G. Guo et al., 2025). This indicates that the TBM method plays a more dominant role in emission reduction than the other methods (Chen et al., 2024). For support systems, a composite lining structure is preferred because of its effective control of deformation in hard rock tunnels and long-term durability. Therefore, this study focuses on the TBM method and composite lining structure as case studies. The boundaries during operation include train operation, lighting, and ventilation.

Temporal boundary: Tunnel engineering design primarily influences carbon emissions during the construction and operational phases, encompassing the installation and use of civil, mechanical, and electrical facilities. Therefore, this study focuses exclusively on these two stages. The typical operational lifespan of a tunnel is approximately 100 years.

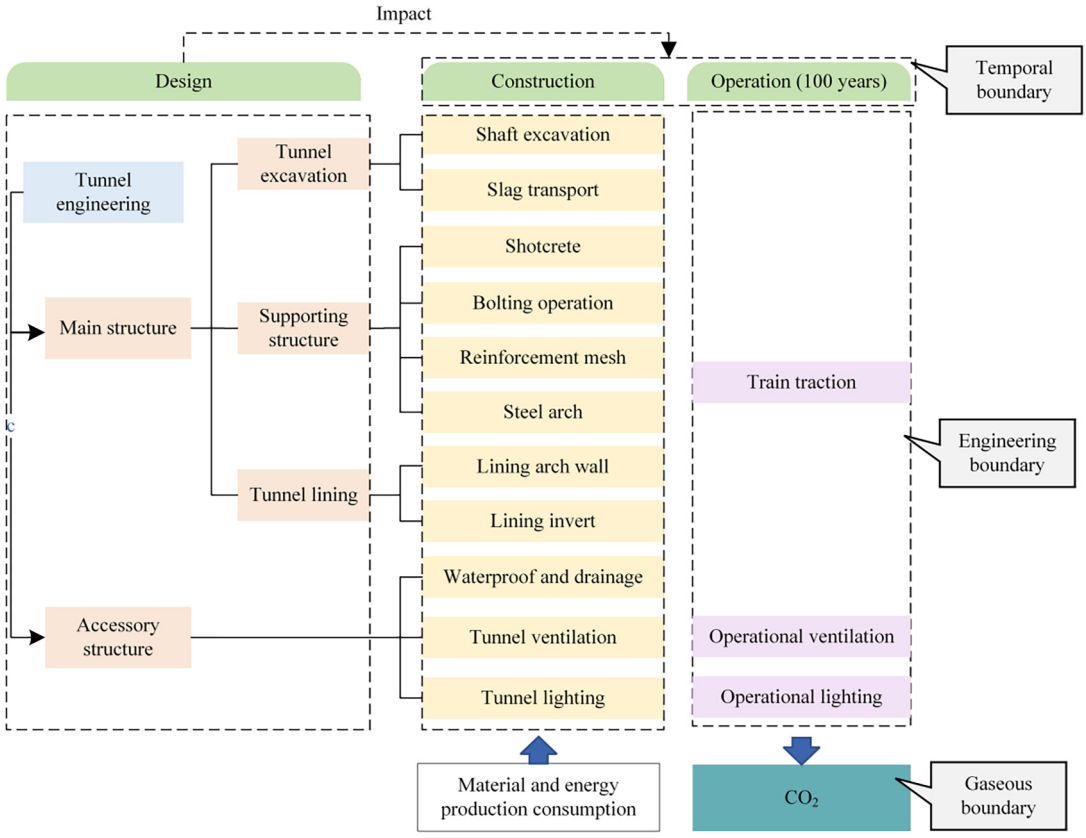

Fig. 2. Tunnel engineering structure decomposition and carbon emission boundaries.

The tunnel engineering carbon emission boundaries are illustrated in Fig. 2.

4 Analysis of the relationship between LDEs and carbon footprint

4.1 DSM-CF model

DSM is a structured modeling tool that represents elements and their interactions within a system. It abstracts complex logical relationships using a matrix format, enhances the process description, and performs iterative analysis (Fazeli & Peng, 2022). A DSM-CF model is proposed to clarify the coupled relationship between LDEs and their impact on carbon emissions (He et al., 2023). In this model, the rows represent the LDEs, whereas the columns encompass the LDEs and associated carbon emission information. The diagonal entries of the DSM represent the LDEs, and the off-diagonal elements indicate the connections between the LDEs, reflecting the transmission and reasoning of the design information. The right-hand side of the DSM shows the influence of the tunnel engineering LDEs on the carbon emissions, as shown in Fig. 3, and the DSM-CF flowchart is shown in Fig. 4.

The DSM-CF model steps are as follows:

Step 1: Define a set of LDEs consisting of n LEDs and construct a matrix based on the DSM-CF model, where k is the carbon footprint of tunnel engineering.

Step 2: Define i and j as the i-th and j-th LDE, respectively. Identify the interaction relationship between LDEs (x, i) and document it using the DSM-CF model. If $i = j$, skip this step and proceed directly to the next step.

Step 3: If $j < n + 1$, increment j by one and return to Step 2. Continue assessing the relationship between LDEs (x, i) and (x, j), cycling through Steps 2–5 until $j = n + 1$.

Step 4: Evaluate whether the LDEs influence the carbon footprint of tunnel engineering. If an impact relationship exists, label it accordingly.

Step 5: Check if $i < n + 1$. If so, increment i by 1, reset j to 1, and return to Step 3 to continue the process until completion.

4.2 Analysis of the relationship between LDEs and carbon footprint based on DSM-CF

4.2.1 Identification of tunnel engineering LDEs

This study introduces the concept of "design scenarios", which integrate lifecycle-related LDEs with design solutions to enhance design comprehensiveness. This approach incorporates the interactions between tunnel design and carbon emissions into a low-emission design framework. The information considered in these design scenarios is categorized into design, construction, and operational information based on the characteristics of the carbon-emitting activities. Through a comprehensive review of the literature on carbon emissions in tunnel engineering,

DSM model									DSM-CF model											
	Low-carbon design elements								Construction carbon footprint (CF_c)						Operational carbon footprint (CF_o)					
	x_1	x_2	x_3	x_4	x_5	x_6	x_7	⋯	CF_{c1}	CF_{c2}	CF_{c3}	CF_{c4}	CF_{c5}	⋯	CF_{o1}	CF_{o2}	CF_{o3}	CF_{o4}	CF_{o5}	⋯
x_1	*					●		⋯			●			⋯			●			⋯
x_2		*			●			⋯		●		●		⋯		●				⋯
x_3			*					⋯						⋯					●	⋯
x_4				*		●		⋯		●				⋯						⋯
x_5		●			*			⋯					●	⋯		●				⋯
x_6					●	*		⋯			●			⋯				●		⋯
x_7			●				*	⋯	●					⋯	●					⋯
⋯			●					*						⋯						⋯

Fig. 3. Sample DSM-CF model.

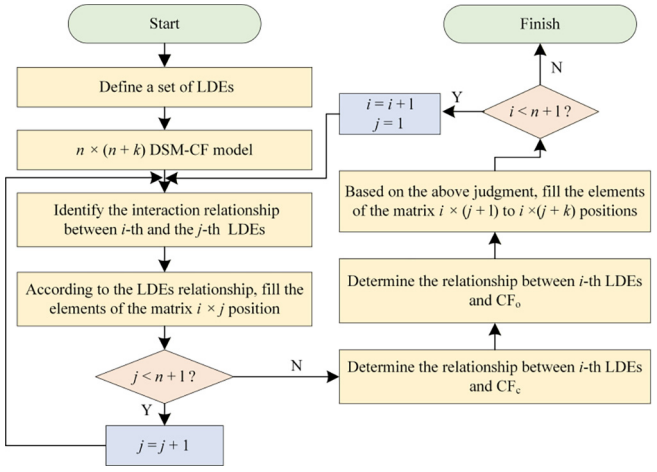

Fig. 4. DSM-CF model flowchart.

this study identifies and organizes the LDEs corresponding to these three dimensions, as listed in Table 1.

4.2.2 Relationship between LDEs and carbon footprint

The grade of the surrounding rock affects the excavation method (Liu et al., 2016). The tunnel length, section shape, and radius influence the volume of the excavation and support area, thereby affecting both energy consumption and material usage. The surrounding rock grade, burial depth, and span determine the structural strength requirements and material usage of a support system. Poor rock stability often necessitates a thicker lining and reduced spacing between the bolts and steel frames, thereby increasing the use of high-carbon materials such as concrete and steel (Guo et al., 2023). The support type, sprayed concrete rebound rate, and material loss during construction directly impact resource waste (Golser et al., 2022). Variations in the base angle alter the support area of the arch walls and inversion in the secondary lining, further influencing emissions. The surrounding rock grade affects the water inflow; a higher inflow requires more drainage pipes and enhanced drainage equipment, leading to increased carbon emissions. The tunnel structure and support type also influence the pipe spacing, further impacting emissions. For waterproofing, the type and thickness of the material are the major elements that influence the emissions. Different materials and thicknesses must be balanced to optimize the waterproofing effectiveness while minimizing carbon emissions.

Ventilation and lighting significantly influence carbon emissions during tunnel construction and operation. The ventilation duration affects energy consumption, whereas train speed and piston wind can enhance natural ventilation, thereby potentially reducing the need for mechanical systems. However, high train speeds can increase traction energy use. The diameter and efficiency of the ventilation ducts further affect the emissions. The lighting energy consumption depends on the power density and duration, and the timings of the ventilation, lighting, and train operations are closely interrelated and influenced by the designed service life of the tunnel.

Through this analysis, the relationship between tunnel LDEs and their impact on carbon emissions is visualized, as shown in Fig. 5.

5 Quantification of the relationship between LDEs and carbon emissions

This study develops a quantitative relationship model between LDEs and carbon emissions to reveal the driving mechanism through which tunnel design influences emissions, rather than providing precise measurements of absolute quantities. Based on the DSM-CF model analysis, this study emphasizes the structural carbon sink effect of key LDEs, simplifying construction machinery, auxiliary materials, and other non-controlling factors. To eliminate uncer-

Table 1
Identification of LDEs of railway tunnel engineering.

Scenario	Element	Abbre.	Source
Design information	Rock mass rating	RMR	Huang et al. (2020)
	Tunnel inflow	Q_w	Rodríguez et al. (2024)
	Section shape	Shp	Xu et al. (2023)
	Sectional area	S	
	Length	L	Xu et al. (2019b)
	Outer contour radius	R	Pritchard and Preston. (2018)
	Slope	i	Xu et al. (2023)
	Burial depth	H	Xu et al. (2019b); Cornet et al. (2018)
	Span	S_p	Ma et al. (2023)
	Support form	SF	Xu et al. (2021)
	Lining thickness	t	Tien et al. (2020); Xu et al. (2021)
	Bolt type	BT	Xu et al. (2021)
	Bolt spacing	l_h 、l_z	
	Bolt length	l_b	
	Frame spacing	w_{sf}	
	Steel mesh spacing	w_{rfm}	
	Base angle	θ	Chen et al. (2024)
	Diameter drain	d_{dra}	Li et al. (2018)
	Diameter pacing	b_{pipe}	
	Thickness of waterproof plate	t_{dra}	Wu et al. (2023)
	Ventilation method	V_M	Guo et al. (2016)
	Ventilation type	V_T	
	Ventilation equipment selection	V_E	
	Fan power	P_v	Zhou et al. (2020)Wang et al. (2023)
	Duct diameter	d_{duct}	
	Single head ventilation length	l_d	
	Luminaire type	C_L	Doulos et al. (2020)Zhao et al. (2021)
	Luminaire layout spacing	b	
Construction information	Excavation method	m_{exc}	Xu et al. (2019a); Xu et al. (2023)
	Material type	C_m	Sun and Park (2020)
	Mechanical excavation electrical	E_{exc}	Wang et al. (2022)
	Average rate of advance	ARA	Zhao et al. (2022)
	Mechanical excavation performance	r	Yi et al. (2016)
	Slag transport power	P_{slag}	Xu et al. (2023)
	Concrete rebound rate	ω_{re}	Fang et al. (2021)Jian et al. (2024)
	Concrete wear rate	ω_{we}	
	Concrete consumption	V_{con}	Liu et al. (2024); Shi et al. (2024); Xu et al. (2021).
	Bolt consumption	M_{bo}	
	Steel arch consumption	M_{sf}	
	Steel mesh consumption	M_{rfm}	
	Drain pipe consumption	M_{dra}	Hopf et al. (2022)
	Waterproof material consumption	M_{wat}	Dammyr et al. (2014)
	Water treatment energy consumption	E_{wat}	Rodríguez and Pérez (2020)
	Energy consumption of ventilation	E_{ven}	Zhang et al. (2018)Guo et al. (2016)
	Mechanical and equipment performance	η	
	Energy consumption of lighting	E_{lig}	Song et al. (2024b)
Operation information	Lighting time	T_{lig}	Song et al. (2024b)
	Lighting power density	P_{lig}	Song et al. (2024b)
	Ventilation time	T_{ven}	Zhou et al. (2020)
	Train speed	v_T	Pritchard and Preston (2018)
	Wind velocity	v_m	Zhou et al. (2020)
	Design life	T	Aldrian et al. (2022)

tainty and highlight the coupling mechanism between LDEs and carbon emissions, conditions are defined through four idealized assumptions: using benchmark values of geotechnical parameters recommended by specifications, setting the standard construction period based on technical guidelines, configuring standardized support materials according to design load requirements, and applying a defined energy efficiency threshold (Chen et al., 2024).

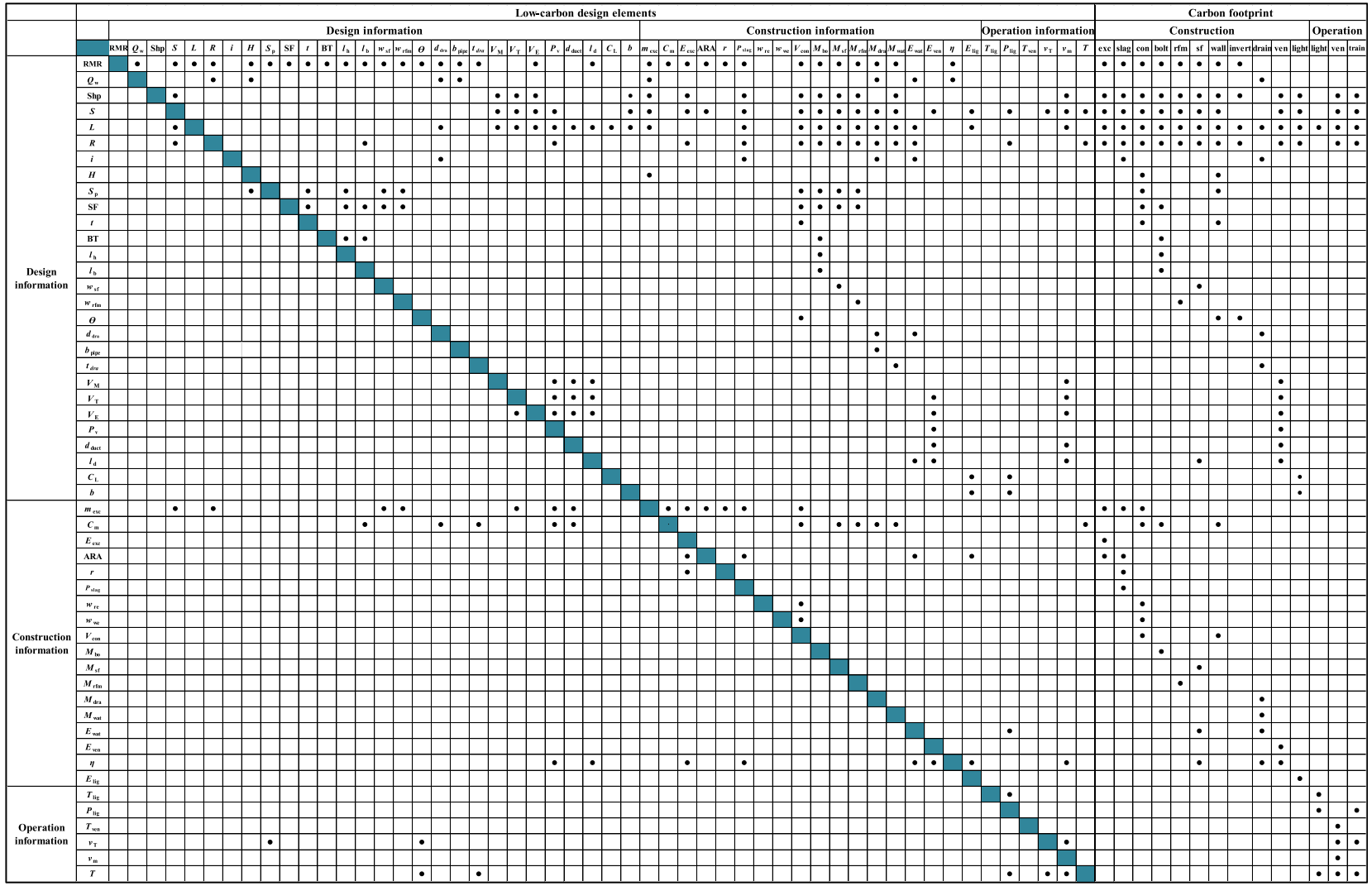

Note: The specific meanings of symbols are listed in Table 1.

Fig. 5. DSM-CF based tunnel engineering carbon emission impact relationship analysis.

Table 2
RMR system rock mass quality classification and engineering parameters (China Railway, 2018).

RMR	Grade	Gravity density (kN/m^3)	Speed (extension meter/d)
100–81	I	>26.5	7.67–8.33
80–61	II		12–14
60–41	III	26.5–24.5	13.3–16
40–21	IV	24.5–22.5	10–11
<21	V	<22.5	

5.1 LDEs and construction carbon emissions

The quantitative relationship between the LDEs and carbon emissions during tunnel construction (CE_c) can be represented as follows:

$$CE_c = \sum_{k=1}^{K} (f(x_{i,k}) \times EF_k), \tag{1}$$

where K is the number of carbon footprints in the construction stage, $f(x_{i,k})$ is the influence function of the i-th design element on the resource consumption of the k-th carbon footprint, and EF_k is the carbon emission factor associated with the k-th carbon footprint.

5.1.1 Tunnel shaft excavation carbon emissions

Carbon emissions from TBM excavation are both the energy consumption during tunneling and carbon emissions generated by the mechanical cutting head.

(1) TBM tunneling energy consumption carbon emissions:

Tunneling is the process of the rotating disk tool of a TBM cutting through rock (She et al., 2023). The required specific energy depends on the geomechanical characteristics of the rock mass. Xue et al. (2018) proposed a calculation formula for specific energy, as follows:

$$S_e = \frac{F_p + 2\pi T_p}{\pi R^2 P}, \tag{2}$$

where S_e is the specific energy (MJ/m^3), F_p is the thrust (kN), T_p is the torque (kN·m), R is the radius of the tunnel contour (m), and P is the penetration (mm/r). The thrust and torque vary with the surrounding rock grade, leading to changes in the specific energy. However, during the design stage, data availability is limited, making the empirical models more accessible (Kim et al., 2020), as follows:

$$E_e = 0.277 S_e/\eta_T = 0.277 \times 80 \exp\left(\frac{RMR - 100}{RMR - 1}\right)/\eta_T, \tag{3}$$

where E_e is the electrical energy consumed by TBM excavation (kW·h/m^3), 0.277 is the conversion coefficient between kW·h and MJ, and η_T is the rate of energy loss during TBM tunneling. RMR refers to the rock mass quality classification coefficient (Zhao et al., 2022), as listed in Table 2.

During tunnel excavation, the TBM can experience downtime, resulting in standby energy consumption (E_0), which is generally E_0 = 5000 kW·h/d (Richard & Celada, 2012). Therefore, the electricity required for tunnel shaft excavation, E_{boring} (kW·h/linear meter), is calculated as follows:

$$E_{boring} = E_e \times S + \frac{E_0}{v_{AR}} = 0.277 \times 80 \exp\left(\frac{RMR - 100}{RMR - 1}\right)/\eta_T \times \pi R^2 + \frac{E_0}{v_{AR}}, \tag{4}$$

where S is the tunnel excavation area (m^2) and v_{AR} is the average rate of TBM tunneling (linear meter/d), and the value is listed in Table 2.

The calculation of carbon emission is as follows:

$$CE_{boring} = EF_e \times E_{boring} \times (L_f - L_o), \tag{5}$$

where CE_{boring} is the energy consumption carbon emissions of the TBM with a tunnel length from L_o to L_f (kg), and EF_e is a CO_2 emission factor for electricity (kg CO_2e/kW·h).

(2) TBM cutting tool consumption carbon emissions:

The consumption of the TBM cutting tool is as follows (Farrokh, 2021):

$$C_C = \frac{1000}{L_{CR} \times V_{exc}} = (0.992 \times CAI \times n_{RPM} \times N_{cutting})/(d_{cutting} \times v_{PR} \times 2R), \tag{6}$$

where C_C is the tool consumption (1/1000 m^3); L_{CR} is the maximum rolling distance of the tool (m); V_{exc} is the excavation volume per 1 m rolling plate (m^3/linear meter); and CAI is the Cerchar Abrasivity Index (Alber et al., 2014), the values of which are listed in Table 3. n_{RPM} is the cutter head revolution (RPM) (r/min), $N_{cutting}$ is the number of tools on the cutter head, $d_{cutting}$ is the tool diameter (inch), and v_{PR} is the boring machine drilling rate (m/h).

If the replaced cutter head is not recycled, its carbon emissions per meter are calculated as follows:

$$CE_{cutting} = EF_{cutting} \times \frac{C_C}{1000} \times m_C \times \pi R^2 \times (L_f - L_o), \tag{7}$$

where m_C is the tool mass (kg), $CE_{cutting}$ is the carbon emission volume consumed by the tool (kg), and $EF_{cutting}$ is the CO_2 emission factor for the tool (kg CO_2e/kg).

The carbon emissions, CE_{exc} (kg), from tunnel excavation are calculated as follows:

Table 3
Range of CAI values.

Abrasion grade	Extremely low	Very low	Low	Intermediate	High	Very high	Extremely high
CAI (10^{-1}mm)	0.1–0.4	0.5–0.9	1.0–1.9	2.0–2.9	3.0–3.9	4.0–4.9	>5

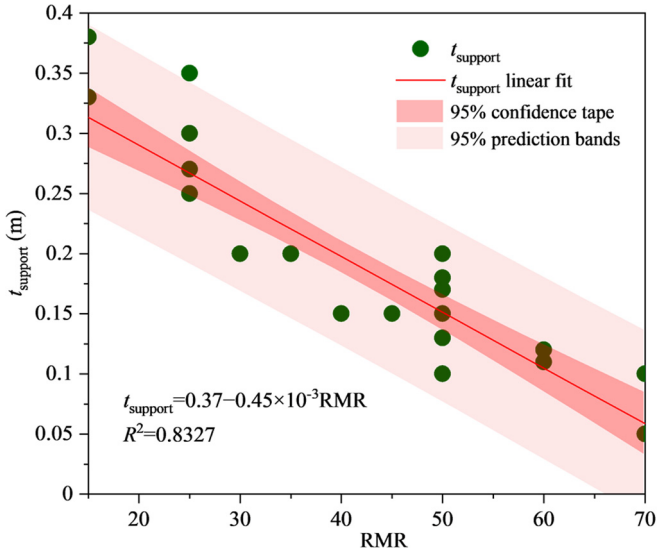

Fig. 6. Correlation between the surrounding rock grade and shotcrete thickness.

$$CE_{exc} = CE_{boring} + CE_{cutting}. \quad (8)$$

5.1.2 Slag transport carbon emissions

The calculation of carbon emissions from tunnel slag transport is as follows:

$$\begin{aligned} CE_{slag} &= EF_e \times P_{slag}(L_f - L_o) \\ &= EF_e \times r \times \pi R^2 \times \rho_r \times (0.075(L_o + L_f) \\ &\quad + 3.75i \times L) \times (L_f - L_o), \end{aligned} \quad (9)$$

where CE_{slag} is the slag transport carbon emission (kg); P_{slag} is the power required by the conveyor belt (kW); r is the maximum excavation performance (m/h), where r = 5 m/h; ρ_r is the density of the surrounding rock (kN/m^3), where the values are listed in Table 2; i is the slope (%).

5.1.3 Tunnel shotcrete carbon emissions

Tunnel shotcrete consumption includes the design amount, rebound amount, and process loss (Fang et al., 2021). These quantities are derived from budget quotas for railway engineering and tunnel design specifications (National Railway Administration of the People's Republic of China (NRA), 2017).

(1) Design dosage of the shotcrete.

The initial concrete spray thickness ranges from 0.05 m (for RMR > 65) to 0.3 m (for RMR < 30). The thickness of the concrete injection is related to the surrounding rock grade (Fig. 6), as expressed in Eq. (10), and the calculation of the concrete design dosage is expressed in Eq. (11).

$$t_{support} = 0.37 - 0.45 \times 10^{-3}\text{RMR}, \quad (10)$$

$$V_{de\text{-}con,support} = \int_{R\text{-}t_{support}}^{R} \pi dR, \quad (11)$$

where $t_{support}$ is the initial spraying thickness of concrete (m) and $V_{de\text{-}con,support}$ is the design quantity of concrete per unit length (m^3/linear meter).

(2) Resilience of the shotcrete.

The formula for calculating the concrete resilience in tunnel engineering is as follows:

$$V_{re\text{-}con,support} = V_{de\text{-}con,support} \times \omega_{re}/(1 - \omega_{re}), \quad (12)$$

where $V_{re\text{-}con,support}$ is the rebound volume of shotcrete (m^3) and ω_{re} is the rebound rate of the shotcrete, where the value is set as 16% (Alkan et al., 2021).

(3) Loss during concrete construction.

Concrete losses, including transport delays, pipe blockages during pumping, and residual concrete left in the pipes after pouring, are typically estimated to be 2%. The actual concrete consumption is determined using Eq. (13), and the carbon emissions are calculated using Eq. (14).

$$V_{con,support} = (V_{de\text{-}con,support} + V_{re\text{-}con,support}) \times (1 + 2\%), \quad (13)$$

$$CE_{con,support} = V_{con,support} \times EF_{con} \times (L_f - L_o), \quad (14)$$

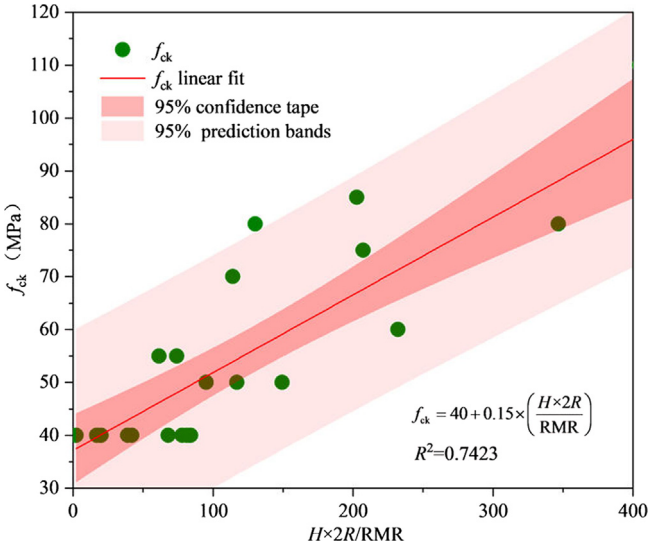

Fig. 7. Correlation between $H \times 2R$/RMR and f_{ck}.

where $V_{con,support}$ is the actual shotcrete consumption (m^3/-linear meter), $CE_{con,support}$ is the shotcrete carbon emissions (kg), and EF_{con} is the concrete carbon emission factor (kg CO_2e/m^3). The carbon emission factor of concrete depends on its compressive strength (f_{ck}), and its linear relationship is as follows (Chen et al., 2024):

$$EF_{con} = 124 + 5.5f_{ck}, (7 \le f_{ck} < 60). \quad (15)$$

The determination of the concrete strength is influenced by factors such as H, R, and RMR. $\frac{H\times 2R}{RMR}$ is a stress index for tunnel supports (Rodríguez et al., 2024), indicating that a higher ratio corresponds to a greater f_{ck} (Fig. 7). Therefore, f_{ck} can be calculated as follows:

$$f_{ck} = 40 + 0.15 \times \left(\frac{H \times 2R}{RMR}\right). \quad (16)$$

5.1.4 Tunnel bolts carbon emissions

The tunnel bolt consumption is calculated using Eq. (17). The carbon emissions calculation for the tunnel lining bolt is given by Eq. (18).

$$M_{bo,support} = l_b \frac{A_{LS}}{l_h \times l_z} \times m_{bo} = l_b \times C_{RMR} \times 2\pi\sqrt{\frac{S}{\pi}}\Big/(l_h \times l_z) \times m_{bo}, \quad (17)$$

$$CE_{bo,support} = M_{bo,support} \times EF_{bo,support} \times (L_f - L_o), \quad (18)$$

where $M_{bo,support}$ is the total mass (kg/linear meter), l_h is the horizontal spacing between bolts (m), l_z is the vertical spacing between bolts (m), l_b is the length of a single bolt (m), m_{bo} is the mass of a unit bolt (kg/m), $CE_{bo,support}$ is the carbon emission of the bolt (kg), $EF_{bo,support}$ is the carbon emission factor of a bolt (kg CO_2e/kg), and C_{RMR} is the bolt adjustment factor depending on the surrounding rock properties. If RMR > 30 and no support is present, then $C_{RMR} = 0.75$, and if RMR ≤ 30, then $C_{RMR} = 1.0$.

Based on the loose ring theory (Yin et al., 2023), the bolt length l_b should satisfy the following:

$$l_b \ge K_s l_{b1} + l_{b2} + l_{b3}, \quad (19)$$

where K_s is the safety factor, with a typically value of 1.5; l_{b1} is the depth of the loosening ring, confirmed by a field test, with a thickness of 0.8–1.1 m; l_{b2} is the anchoring length, which ranges from 1.2–1.6 m; l_{b3} is the exposed length of the bolt, which ranges from 0.1–0.2 m; therefore the optimal bolt length is 2.5–3.5 m.

The bolt spacing depends on the rock mass quality grade and can be calculated as follows:

$$l_{h,z} = 0.5 + 2.5\frac{RMR - 20}{65}, \quad (20 < RMR \le 85). \quad (20)$$

5.1.5 Tunnel supporting steel fabric carbon emissions

Based on the TB 10003—2016 "Code for Design of Railway Tunnels" (NRA, 2016), a steel mesh is not used in Class I and II surrounding rock. The quantities of steel mesh per linear meter for Class III and IV/V surrounding rocks are given by Eq. (21), and the carbon emissions from the steel mesh support are expressed in Eq. (22).

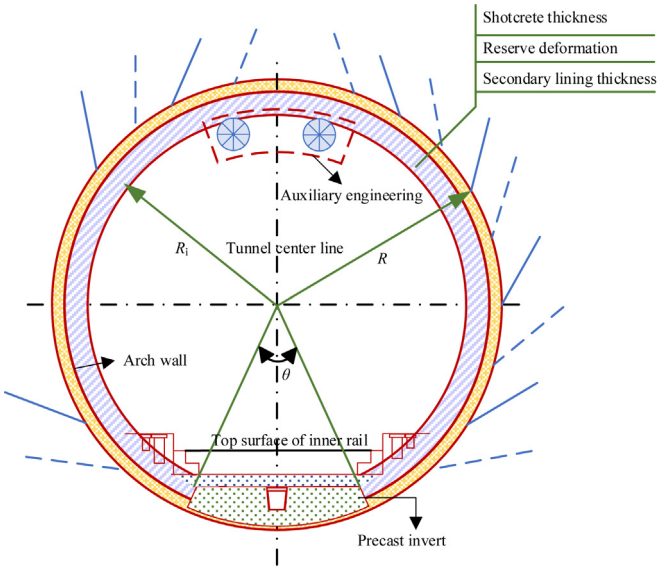

Fig. 8. Tunnel lining structure.

$$M_{rfm,support} = \left(2 \times C_{RMR} \times 2\pi\sqrt{\frac{S}{\pi}}\Big/ w_{rfm}\right) \times m_{rfm}, \quad (21)$$

$$CE_{rfm,support} = M_{rfm,support} \times EF_{rfm,support} \times (L_f - L_o), \quad (22)$$

where $M_{rfm,support}$ is the mass of the steel mesh (kg); m_{rfm} is the mass of the unit reinforcement (kg/m); w_{rfm} is the spacing of the steel mesh (m), which ranges from 0.15 to 0.30 m; $CE_{rfm,support}$ is the carbon emissions of steel mesh; $EF_{rfm,support}$ is the carbon emission factor of steel fabric (kg CO_2e/kg).

5.1.6 Tunnel supporting steel frame carbon emissions

The steel consumption is calculated using Eq. (23), and the carbon emissions of steel frame supports in tunnel engineering are given by Eq. (24).

$$M_{sf,support} = C_{RMR} \times 2\pi\sqrt{\frac{S}{\pi}}\Big/ w_{sf} \times m_{sf} + m_b, \quad (23)$$

$$CE_{sf,support} = M_{sf,support} \times EF_{sf,support} \times (L_f - L_o), \quad (24)$$

where $M_{sf,support}$ is the mass of the steel mesh (kg/linear meter), m_{sf} is the mass of the unit reinforcement (kg/m), w_{sf} is the spacing of the steel mesh (m), m_b is the weight of the joint (kg), $CE_{sf,support}$ is the carbon emissions of the

Table 4
Reserved deformation of surrounding rock.

Surrounding rock grade	Tunnel span (m)		
	Small span	Midspan	Long-span
II		0–30	30–50
III	10–30	30–50	50–80
IV	30–50	50–80	80–120
V	50–80	80–120	120–170

steel frame (kg), and $EF_{sf,support}$ is the carbon emission factor of steel frame (kg CO_2e/kg). During the design process, the spacing of the steel frame is typically based on the quality of the surrounding rock. For Class IV surrounding rock, the spacing is typically between 1.0 and 1.2 m, while for Class V, it is generally between 0.6 and 0.8 m (NRA, 2016).

5.1.7 Tunnel lining arch wall carbon emissions

The tunnel lining consists of arch walls and inverts, as shown in Fig. 8.

(1) Arch wall design carbon emissions.

The arch wall of the tunnel lining consists of an arch wall design and reserved deformation backfill. The carbon emissions from the arch wall are calculated as follows:

$$CE_{de\text{-}walls,lining} = \frac{1}{2}\left(\int_{\alpha}^{\beta}\left(R_i + t_{lining}\right)^2 d\theta - \frac{1}{2}\int_{\alpha}^{\beta} R_i^2 d\theta\right) \times (EF_{con} + \rho_s EF_{rebar}) \times (L_f - L_o), \quad (25)$$

where $CE_{de\text{-}walls,lining}$ is the carbon emission of the arch wall lining design (kg), t_{lining} is the lining thickness (m), R_i is the inner diameter of the tunnel (m), ρ_s is the reinforcement ratio of steel bars, θ is the inner angle of the concrete base referred to Fig. 8, and EF_{rebar} is the carbon emission factor of lining steel bars (kg CO_2e/m^3).

(2) Reserve deformation of the surrounding rock of backfilled concrete carbon emissions.

The unconverted portion of the reserved deformation is backfilled with concrete. Designers use one-third of the reserved deformation value to calculate the required volume of molded concrete for backfilling, as follows:

$$CE_{backfill\text{-}walls,lining} = \frac{1}{3}\int_{\alpha}^{\beta} R_i d\theta \times C \times EF_{con} \times (L_f - L_o), \quad (26)$$

where C is the reserved deformation of the surrounding rock (m), based on TB 10003—2016 "Code for Design of Railway Tunnels" (NRA, 2016), and the values are listed in Table 4. $CE_{backfill\text{-}walls,lining}$ represents the carbon emissions generated by the resilience of the lining arch wall (kg).

5.1.8 Tunnel lining invert carbon emissions

A tunnel invert is generally prefabricated and its carbon emissions are calculated as follows:

$$CE_{invert,lining} = \left(\pi R_i^2 \times \frac{\theta}{360}\right) - R_i^2 \times \sin\left(\frac{\theta}{2}\right) \times \cos\left(\frac{\theta}{2}\right) \times (EF_{con} + \rho EF_{rebar}) \times (L_f - L_o), \quad (27)$$

where $CE_{invert,lining}$ is the carbon emission of the lining invert (kg).

5.1.9 Tunnel waterproof and drainage system carbon emissions

Carbon emissions from anti-drainage systems in tunnel engineering primarily arise from drainage systems, construction of waterproofing systems, and tunnel anti-slope drainage measures.

(1) Drainage system construction carbon emissions.

In tunnel engineering, a drainage system primarily comprises side ditches, central ditches, and circular drainage pipes. Carbon emissions are mainly influenced by the material, diameter, and laying length of the drainage pipes and are calculated as follows:

$$CE_{dra} = 2\pi d_{central} \times L \times \rho_{central} EF_{central} + \pi d_{side} L \times \rho_{side} EF_{side} + \pi d_{pipe} \times \frac{L}{b_{pipe}} \times \rho_{pipe} EF_{pipe}, \quad (28)$$

where CE_{dra} is the drainage pipe layout of carbon emissions (kg); d_{side}, $d_{central}$, and d_{pipe} are the diameters of the measuring ditch, central ditch, and circumferential drainage pipe (m), respectively; b_{pipe} is the layout spacing of the circumferential pipe (m); $\rho_{central}$, ρ_{side}, and ρ_{pipe} are the densities of the related materials, respectively; $EF_{central}$, EF_{side}, and EF_{pipe} are the carbon emission factors of the related materials, respectively (kg CO_2e/kg).

(2) Waterproof system construction carbon emissions.

The waterproofing system of a tunnel project depends on the waterproofing material and laying area, and the carbon emissions are calculated as follows:

$$CE_{waterproof} = 2\pi R \times t_{waterproof} \times EF_{waterproof} \times (L_f - L_o), \quad (29)$$

where $CE_{waterproof}$ represents the carbon emissions for waterproofing systems (kg), $t_{waterproof}$ is the thickness of the material (m), and $EF_{waterproof}$ is the carbon emission factor of the material (kg CO_2e/kg).

(3) Tunnel drainage on the reverse slope carbon emissions.

Tunnel drainage design should consider the slope i, water volume, and layout of pipelines and pump stations. A multi-stage centrifugal pump is used for reverse slope drainage. The electric power of the pump, P_w (kW), is calculated as follows:

$$P_w = \frac{g}{\eta_p}\left(\frac{i}{100} + 10.34\frac{Q_w^2}{d_{dra}^{16/3}}\right)L^2 \times q_L, \quad (30)$$

where η_P is the overall performance of the multi-stage centrifugal clean pump; Q_w is the water inflow of the tunnel (m^3/s); q_L is the specific water flow, generally q_L is 2×10^{-5} m^3/s; g is the acceleration of gravity; d_{dra} is the pipe diameter (m).

The energy consumed by the reverse slope drainage of the tunnel is calculated using Eq. (31), and the carbon emissions are determined using Eq. (32).

$$E_m = t_m \times P_m = \frac{L_f - L_o}{v_{AR}} P_m, \tag{31}$$

$$CE_m = E_m \times EF_e, \tag{32}$$

where t_m is the working time of the machine (h). The calculation of carbon emissions from the ventilation and lighting equipment also uses the Eqs. (31) and (32), with the power parameters determined using Eqs. (33) and (34), respectively.

5.1.10 Tunnel ventilation carbon emissions

The selection of the ventilation scheme in TBM long-distance construction ventilation for railway tunnels is closely related to the air supply volume at the palm surface, the ventilation length of a single head, and the design of the cross passage. The motor power of the axial fan is calculated as follows:

$$P_{ven,const} = 10^{-3} \frac{\lambda Q_V^3}{d_{duct}^5 \eta_F} L, \tag{33}$$

where $P_{ven,const}$ is the motor power of the axial fan (kW), η_F is the overall performance of the fan with a value of 0.8, d_{duct} is the duct diameter (m), λ is the friction factor with a value of 0.024, Q_V is the airflow provided by the ventilation system (m^3/s), and L is the length of the tunnel ventilation section (m).

5.1.11 Tunnel lighting carbon emissions

The tunnel lighting uses n lamps with a power of P_{l1} (W), and the tunnel lighting spacing is b_l (m). Each working face is illuminated using m lamps with a power of P_{l2} (W). Assuming g working faces, the tunnel lighting power consumption $P_{lig,const}$ (kW) is calculated as follows:

$$P_{lig,const} = \frac{np_{l1}}{b} L + m \times g \times p_{l2}. \tag{34}$$

5.2 LDEs and operation carbon emissions

The structural and functional design in tunnel engineering significantly affects the operational energy consumption of a project. Primary considerations include the energy used by train operations, lighting, and ventilation systems. Energy consumption for these components is calculated based on the running time t and running power P_{ri} under different operational states. Therefore, the carbon emissions generated during the tunnel operation are calculated as follows:

$$CE_o = E_{total} \times EF_e = \sum_{j=1}^{J} \int_{t_{si}}^{t_{ei}} P_{ri} dt \times EF_e, \tag{35}$$

where CE_o is the carbon emissions generated during the operation phase (kg), and E_{total} represents the total energy consumption of the j-th module during the operation of t_e–t_s. P_{ri} represents the power of module i-th when it runs in r-th state.

5.2.1 Lighting system operation energy consumption

The calculation of the lighting system energy consumption should consider factors such as natural lighting, control mode, and usage time. If the lighting system lacks an automatic photoelectric control system, the annual energy consumption is calculated as follows:

$$E_{lig,ope} = T \sum_{j=1}^{366} \sum_{i} P_{ij} \times A_i \times t_{ij} + 24 P_p \times A_L, \tag{36}$$

where $E_{lig,ope}$ is the annual energy consumption of the lighting system (kW·h/a); T is the operating years of the tunnel; P_{ij} is the illumination power density value of the j-th day i-th region (W/m^2), which is consistent with the design document; A_i is the lighting area of the i-th region (m^2); t_{ij} is the illumination time of area i-th on the j-th day (h); P_P is the emergency lighting power density (W/m^2); A_L is the total area of the bright area (m^2).

5.2.2 Ventilation system operation energy consumption

The ventilation time for tunnel operation under electric locomotive traction is determined based on the environmental conditions inside the tunnel and the maintenance duration of the skylight, and the annual energy consumption is calculated as follows (NRA, 2024):

$$\begin{aligned} E_{ven,ope} &= T \sum_{j=1}^{366} t_{ven,ope} \times P_{ven,ope} \\ &= T \sum_{j=1}^{366} t_{ven,ope} \times 0.992 K_D \\ &\quad \times \frac{\lambda L K_r^3}{1000 \eta_F \eta_m K_R^3 d_{duct}^5} \left(K_i \left(1 - \frac{v_m}{v_T} \right) \frac{SL}{t_{ven,ope}} \right)^3, \end{aligned} \tag{37}$$

where η_m is the motor efficiency with a value of 0.9–0.95; K_D is the motor capacity safety factor, which is preferably 1.15; η_F is the fan performance, which is generally 0.80; K_R is the air volume distribution coefficient with a value of 0.5; K_r is the air volume distribution correction coefficient with a value of 1.05; K_i is the piston wind correction factor. For operational tunnels with diesel locomotives, a value of 1.1 can be adopted, whereas for those with electric locomotives, a value of 1.0 is appropriate; v_T is the train speed (km/h); v_m is the piston wind speed in the tunnel (m/s); S is the cross-sectional area of the tunnel (m^2); $t_{ven,ope}$ is the daily ventilation time (s).

5.2.3 Train traction energy consumption

Train traction energy consumption is influenced by the work required to overcome resistance and the efficiency of the transmission system (Bai et al., 2009). The transmission efficiency can be utilized to estimate traction energy

Table 5
Design information for the tunnel.

Surrounding rock grade	Length (km)	Initial spray thickness (cm)	Anchor bolt		Reinforcement mesh (cm × cm)	Steel frame
			Length (m)	Interval (m × m)		
II	4.08	5	–	–	–	–
III	5.30	12	2.5	1.5 × 1.5	Above semicircle Φ8, 25 × 25	–
IV	7.99	15	3.0	1.2 × 1.5	Above semicircle Φ8, 25 × 25	Complete ring HW100, 1.8 m/beam
V	4.53	20	3.0	1.2 × 1.2	Φ8, 25 × 25	Complete ring HW150, 0.8 m/beam

Table 6
Carbon emission factor.

Factor	Data	Unit	Data source
EF_e	0.2268	kg CO_2eq/(kW·h)	Climate Change Department of the Ministry of Ecology and Environment of the People's Republic of China (2025)
$EF_{bo,support}$	1.540	kg CO_2eq/kg	Y. Guo et al. (2025)
$EF_{cutting}$	2.596	kg CO_2eq/kg	
$EF_{rfm,support}$	2.310	kg CO_2eq/kg	
$EF_{sf,support}$	2.425	kg CO_2eq/kg	
$EF_{central}$	2.50	kg CO_2eq/kg	Ministry of Housing and Urban-Rural Development of the People's Republic of China (2019)
EF_{side}	1.95	kg CO_2eq/kg	
EF_{pipe}	2.84	kg CO_2eq/kg	
$EF_{waterproof}$	2.38	kg CO_2eq/kg	

consumption by considering the running resistance, as shown in Eqs. (38) and (39) (NRA, 2018).

$$E_{\text{train}} = \int_0^T u_t(t) f_t(v) v(t)/\eta \cdot \mathrm{d}t, \tag{38}$$

$$\begin{cases} f_t(v) = \frac{\rho}{2}\left\{\left[\frac{(v_m - v_T)S}{(S - A_v)} - v_T\right]^2 - (v_m - v_T)^2\right\}A_v + \frac{\rho}{2}(v_m - v_T)^2\left[\beta/(1-\beta)^2\right] \\ \quad (1 - \beta - C_h - C_t)A_v - \frac{\rho l_T}{2(S - A_v)}(w|w|\frac{\lambda}{4}S_t A_v + w'|w'|\frac{\lambda'}{4}S_v S) \\ v_m = v_T \dfrac{-1 + \sqrt{1 + \left(\frac{\xi_m}{K_m} - 1\right)\left(1 \pm \frac{\xi_n v_T'^2}{K_m v_T^2}\right)}}{\frac{\xi_m}{K_m} - 1} \\ \xi_m = 1 + \lambda\frac{L - l_T}{d} + \xi \\ \xi_n = 1 + \lambda\frac{L}{d} + \xi \end{cases}, \tag{39}$$

where E_{train} is traction train single operation energy consumption (kW·h), $u_t(t)$ is the tractive force coefficient at time t with a value of 0.35–0.40, $f_t(v)$ is the traction force of the train at time t (N), and η is the train comprehensive efficiency with a value of 0.85. ρ is the air density (kg/m^3) with a value of 1.29 kg/m^3; A_v is the train section area (m^2); β is the congestion ratio, where $\beta = A_v/S$; C_h is the pressure difference resistance coefficient of the train head, which is generally valued between 0.1 and 0.3; C_t is the pressure difference resistance coefficient of the train tail, which is generally valued between 0.2 and 0.5; w is the natural wind speed, w' is the annular space airflow velocity (m/s), and λ' is the friction coefficient of the train wall with a value of 0.018. d is the average hydraulic diameter (m), S_t is the wet circumference (m), S_v is the wet cycle of the train (m), and K_m is the piston wind action coefficient with a general value of 0.6. ξ_m is the resistance coefficient of the tunnel section excluding the annular space, ξ_n is the total resistance coefficient of the tunnel, ξ is the local resistance coefficient with a value of 0.5, and l_T is the train length (m).

6 Case study

6.1 Engineering background

This case study examined a tunnel project in Southwest China. The tunnel is designed as a single-line, circular cross-sectional tunnel constructed using a TBM with an inner contour radius of 4.4 m. During construction, the normal groundwater inflow was 6693.89 m^3/d, with a peak inflow of 20 093.25 m^3/d. The ventilation system uses a single-head forced ventilation mode operating for 240 min daily. The natural wind speed is 1.5 m/s, and the air density is 0.944 kg/m^3. The design details are listed in Table 5 with data sourced from tunnel engineering design documents. The corresponding carbon emission factors are listed in Table 6.

6.2 Carbon emission calculation

The proposed method was used to calculate carbon emissions based on the design parameters of tunnel engineering, and the calculation results are listed in Table 7.

Table 7
Comparison of carbon emissions for different surrounding rock grades in the tunnel.

Stage	Carbon emissions	Surrounding rock grades (kg CO_2e/linear meter)				Total (t)	Proportion (%)
		II	III	IV	V		
Construction	CE_{exc}	2911.81	2823.06	2755.11	2497.65	61 092.33	20.64
	CE_{slag}	1149.60	1091.56	896.19	777.32	21 147.55	7.14
	$CE_{con,support}$	1099.05	2324.29	3741.46	4717.38	68 037.62	22.98
	$CE_{bo,support}$	–	98.85	370.68	617.80	6281.94	2.12
	$CE_{rfm,support}$	–	97.46	175.43	233.91	3194.28	1.08
	$CE_{sf,support}$	–	–	414.9	1244.7	8951.45	3.02
	$CE_{walls,lining}$	2481.06	2638.29	2961.15	3316.44	62 760.77	20.70
	$CE_{invert,lining}$	1412.22	1462.20	1578.82	1724.59	33 923.42	14.10
	$CE_{waterproof\ and\ drainage}$	276.74	381.58	366.77	223.06	13 669.46	4.62
	$CE_{ven,const}$	194.95	158.40	253.44	316.80	5092.99	1.72
	$CE_{lig,const}$	253.88	253.88	253.88	253.88	5557.51	1.88
Operation	$CE_{lig,ope}$	5600 t					
	$CE_{ven,ope}$	5400 t					
	CE_{train}	2.49×10^6 t					

6.3 Model rationality verification

This study verified the scientific validity of the proposed model in two dimensions. First, it examined the applicability of boundary simplification by analyzing the actual carbon emission characteristics during tunnel construction. Second, it compared the estimated carbon emissions during the construction phase with the actual energy and resource consumption data from the project to validate the reasonableness of the model developed in this study.

6.3.1 Boundary simplification rationality

The actual carbon emission characteristics of tunnel engineering were analyzed and visualized using a pie chart, as shown in Fig. 9.

Figure 9 indicates that a significant concentration pattern exists among the key contributors despite the diverse characteristics of carbon emission sources in tunnel engineering. The carbon sink effect of high-carbon structures accounts for over 80% of the carbon emissions. In the TBM excavation process, which includes 19 subcategories of carbon emission sources (NRA, 2017), there are five main contributors: TBM energy consumption (48.3%), axial flow fan (18.1%), tunnel belt conveyor (15.9%), TBM cutting tool (8.6%), and clean water pump (2.1%). Together, these sources represent 92.7% of the total emissions. Similarly, in the support structure, shotcrete production and application accounted for 87.4% of the carbon emissions, whereas steel consumption constituted 90% of the emissions from the rock bolt system. The impact of other auxiliary machinery and materials remained below 10%, which is significantly lower than the error tolerance threshold for decision support systems in engineering practice. Therefore, it is reasonable to simplify non-major emission sources.

This study independently analyzed TBM quota subitems (ventilation, slag transportation, and water treatment) through systematic reconstruction, avoiding overlap in calculations and ensuring comprehensive coverage of dominant emission sources.

6.3.2 Quantification model for LDEs and carbon emissions validity

This study compared the emissions estimated by the model during the construction phase with those generated from actual energy and resource consumption to verify the effectiveness of the LDE-carbon emission quantification model. The results are shown in Fig. 10, where the red area indicates the allowable deviation range for carbon emissions. Given the uncertainties associated with a long operational phase, carbon emission accounting is complex. Therefore, the verification specifically focused on the prediction accuracy of the model during the construction phase.

Figure 10 shows that both the model estimates and actual values fell within the allowable deviation range, demonstrating the effectiveness of the model in predicting carbon emissions during the construction phase. The observed discrepancies were minor, remaining well within the permissible threshold and aligning with theoretical expectations. These discrepancies primarily stem from the differences between the design assumptions and actual conditions, including geological variability and equipment operating efficiency. All deviations were systematic with no significant outliers, further confirming the validity of the model.

The primary source of deviations in the carbon emission estimation for anchor supports arises from the gap between design specifications and actual engineering practices. Current tunnel design standards specify that anchor supports are unnecessary for Class I and II surrounding rocks. However, designers often add anchors for safety redundancy. Although this enhances structural safety, it complicates the accurate quantification of carbon emissions. Existing models based on standard benchmarks tend to overlook the carbon contribution of these non-standard safety mea-

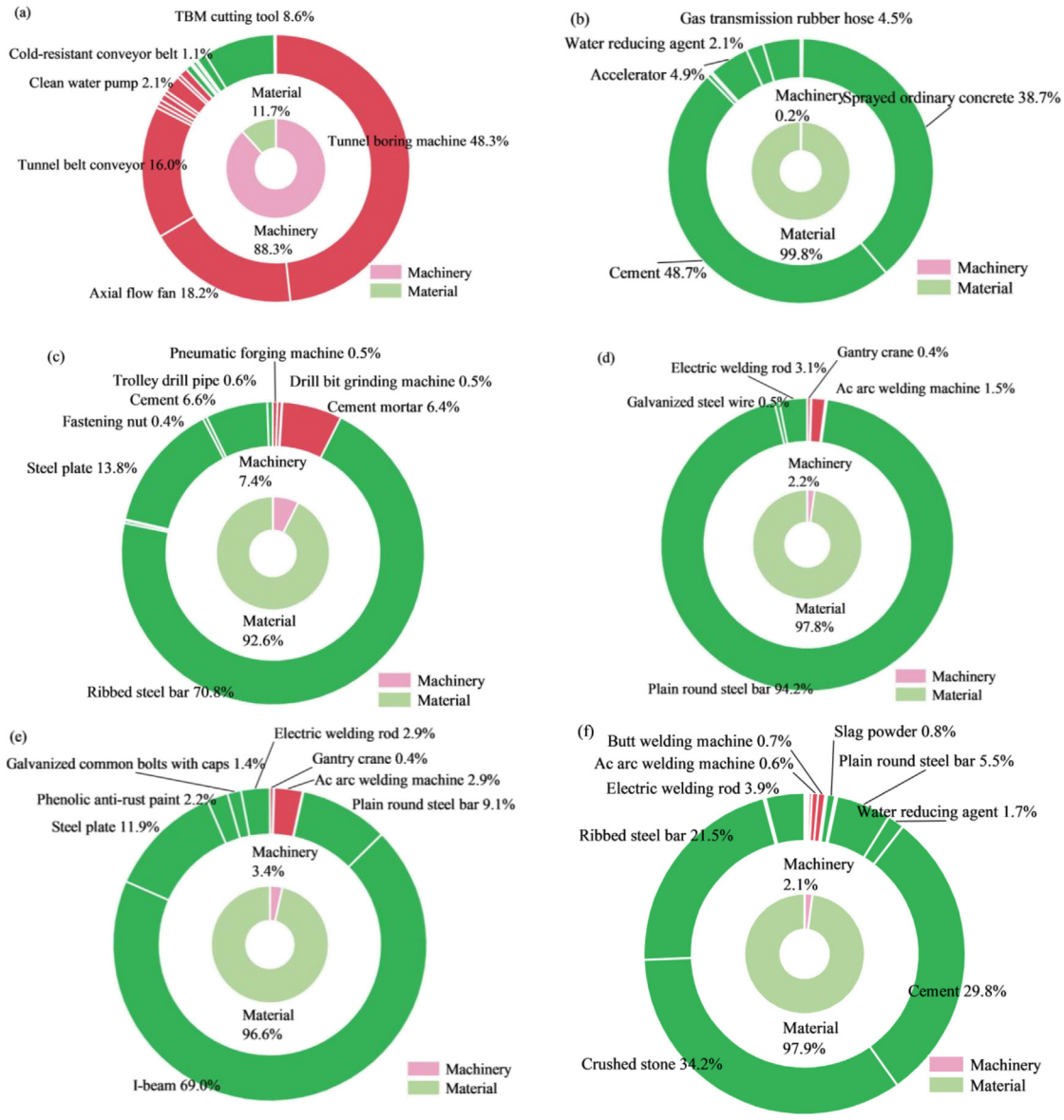

Fig. 9. Actual carbon emission characteristics of the tunnel. (a) CE_{exc}, (b) $CE_{con,support}$, (c) $CE_{bo,support}$, (d) $CE_{rfm,support}$, (e) $CE_{sf,support}$, and (f) $CE_{,lining}$.

sures, resulting in an underestimation. Research indicates that such deviations can account for 8% to 12% of the total emissions, significantly affecting model accuracy.

The difference in carbon emissions from tunnel inverts primarily results from the application of prefabrication technology and C40 reinforced concrete, which often inadequately represents the characteristics of the surrounding rock. Traditionally, this has led to relatively stable carbon emissions despite considerable geological variations, failing to reflect the actual impact of geological conditions. This study incorporated the surrounding rock grade as a key factor affecting concrete strength in the model, revealing that carbon emissions from the invert increase as the surrounding rock grade decreases, producing discrepancies between theoretical calculations and actual carbon emissions.

In addition, the spatiotemporal variability of geological conditions, fluctuations in construction progress, and uncertainties in energy efficiency significantly influence the differences between designed and actual carbon emissions during operation. When tunneling with a TBM, the model simplifies the geotechnical parameters, excavation time, and efficiency using the typical values. Sudden changes in the surrounding rock grade and joint development can alter the energy efficiency of the TBM cutter head, leading to deviations in the excavation energy consumption from design expectations. In addition, during the shotcrete process, misjudging the self-supporting capacity of the surrounding rock often results in over-spraying or under-spraying, causing variations in sprayed thickness and amplifying material consumption. Although the model calculates carbon emissions based on parameters such as the surrounding rock grade and radius, the practical use of high-performance concrete can reduce the support requirements and associated carbon emissions. This results in discrepancies between the theoretical and actual carbon emissions in localized zones. However, the uncertainties

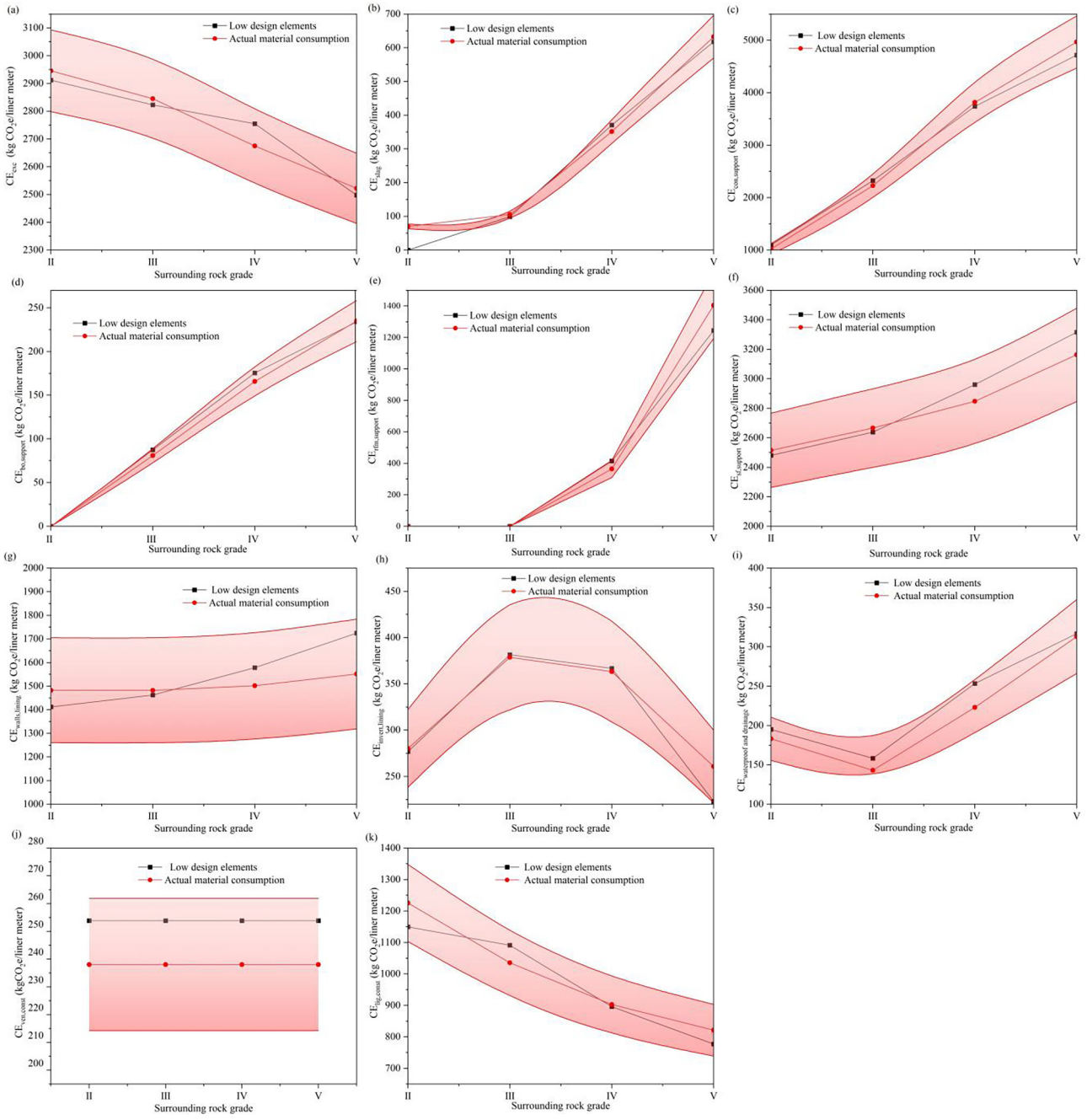

Fig. 10. Comparison of the carbon emission of the tunnel. (a) CE_{exc}, (b) CE_{slag}, (c) $CE_{con,support}$, (d) $CE_{bo,support}$, (e) $CE_{rfm,support}$, (f) $CE_{sf,support}$, (g) $CE_{walls,lining}$, (h) $CE_{invert,lining}$, (i) $CE_{waterproof\ and\ drainage}$, (j) $CE_{ven,const}$, and (k) $CE_{lig,const}$.

arising from parameter coupling continue to create a deviation-control complex.

7 Results and discussion

7.1 Influence of LDEs on carbon emission of tunnel construction

The carbon emissions calculated using the model are shown in Fig. 11. Shotcreting for the primary support contributed the most at 22.98%, followed by arch wall construction in the secondary lining at 20.70%, and electric energy and tool head consumption during tunnel driving at 20.64%. Invert installation accounted for 14.1%, and slag transport contributed 7.14%. The majority of the embedded emissions were concentrated in the tunnel support, lining, and excavation activities, which is consistent with the findings reported by Spyridis and Bergmeister (2024). Collectively, these high-emission processes constituted nearly 85.56% of the total carbon emissions during the construction stage, emphasizing the notably high-carbon footprint associated with tunnel construction.

The primary objective of this study was to analyze the mechanisms by which LDEs influence carbon emissions,

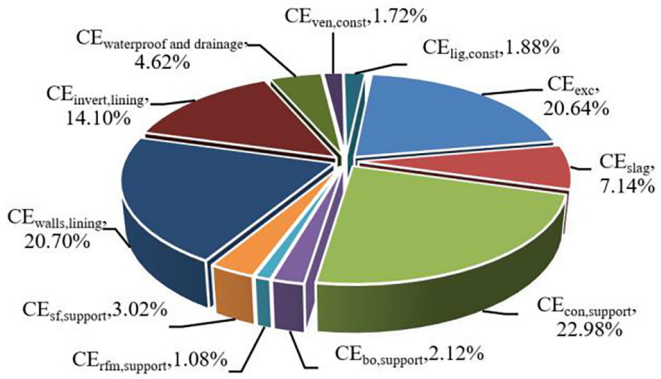

Fig. 11. Carbon emission pie chart.

thereby enabling targeted interventions for carbon reduction. As high-carbon footprint processes dominate the emission system, they have been identified as key intervention targets. Based on the established quantitative relationship model between LDEs and carbon emissions, this study examined high-carbon structural components in tunnel engineering through a multi-parameter coupling analysis. Influence diagrams were constructed to illustrate the relationship between the LDEs and carbon emissions (Figs. 12–17), revealing the nonlinear influence patterns of core LDEs on carbon emissions and providing explicit directional guidance for low-carbon design strategies.

7.1.1 Effects of LDEs on carbon emissions from tunnel shaft excavation

Figure 12 illustrates the influence of RMR and ARA on carbon emissions during TBM construction. As shown in Fig. 12(a), when the surrounding rock grade improved from Class V to Class II, with RMR values ranging from 20 to 80 and ARA values fluctuating between 5 and 15, the carbon emissions varied between 2500 and 3400 kg CO_2e. Low-grade surrounding rock, owing to its loose structure and low compressive strength, reduces the pene-

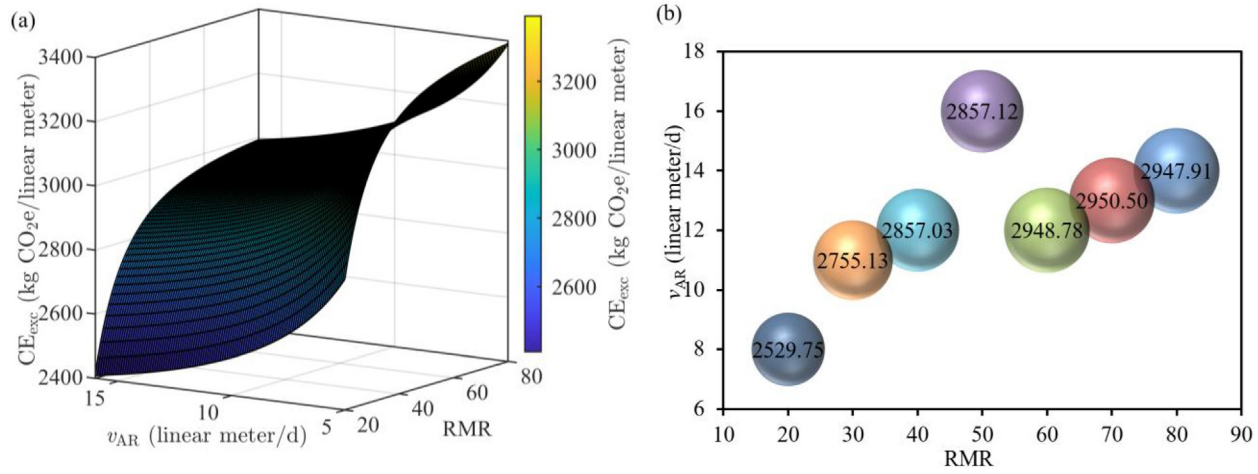

Fig. 12. Effects of ARA and RMR on carbon emissions from tunnel excavation. (a) Relationship between ARA and RMR is not considered, and (b) relationship between ARA and RMR is considered.

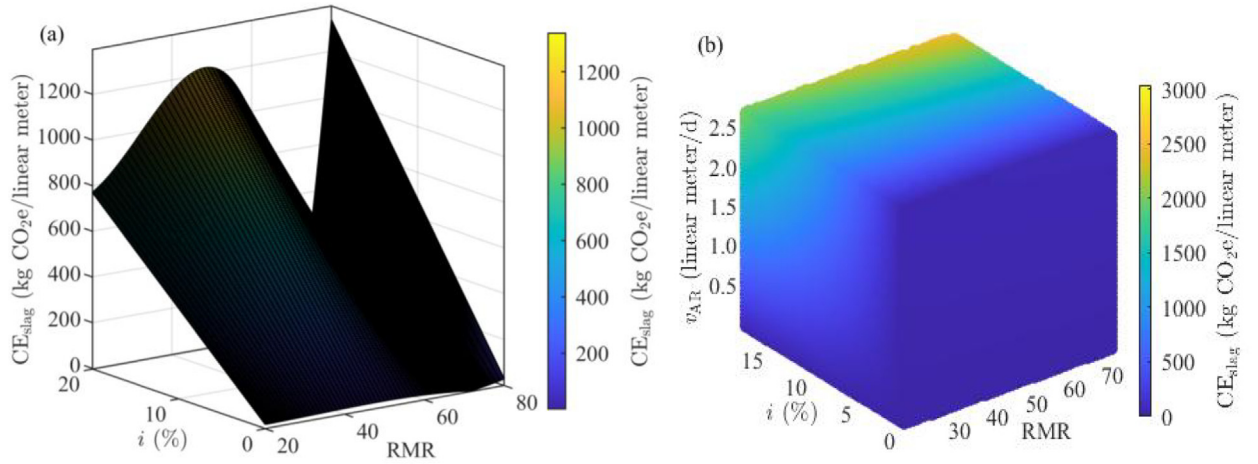

Fig. 13. (a) Effects of RMR and *i* on carbon emissions from tunnel slag transport, and (b) effects of RMR, *i*, and ARA on carbon emissions from tunnel slag transport.

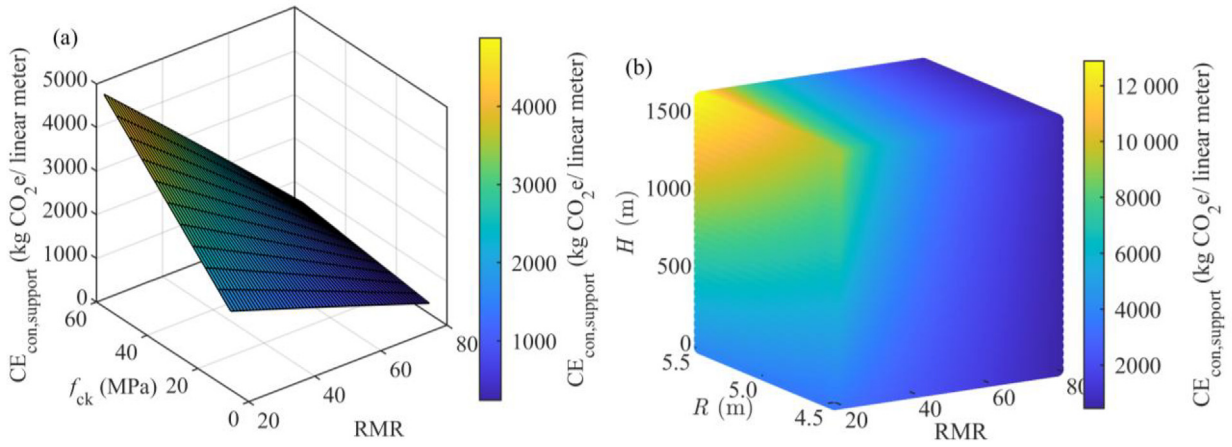

Fig. 14. (a) Effects of RMR and f_{ck} on carbon emissions from tunnel shotcrete, and (b) effects of RMR, R, and H on carbon emissions from tunnel shotcrete.

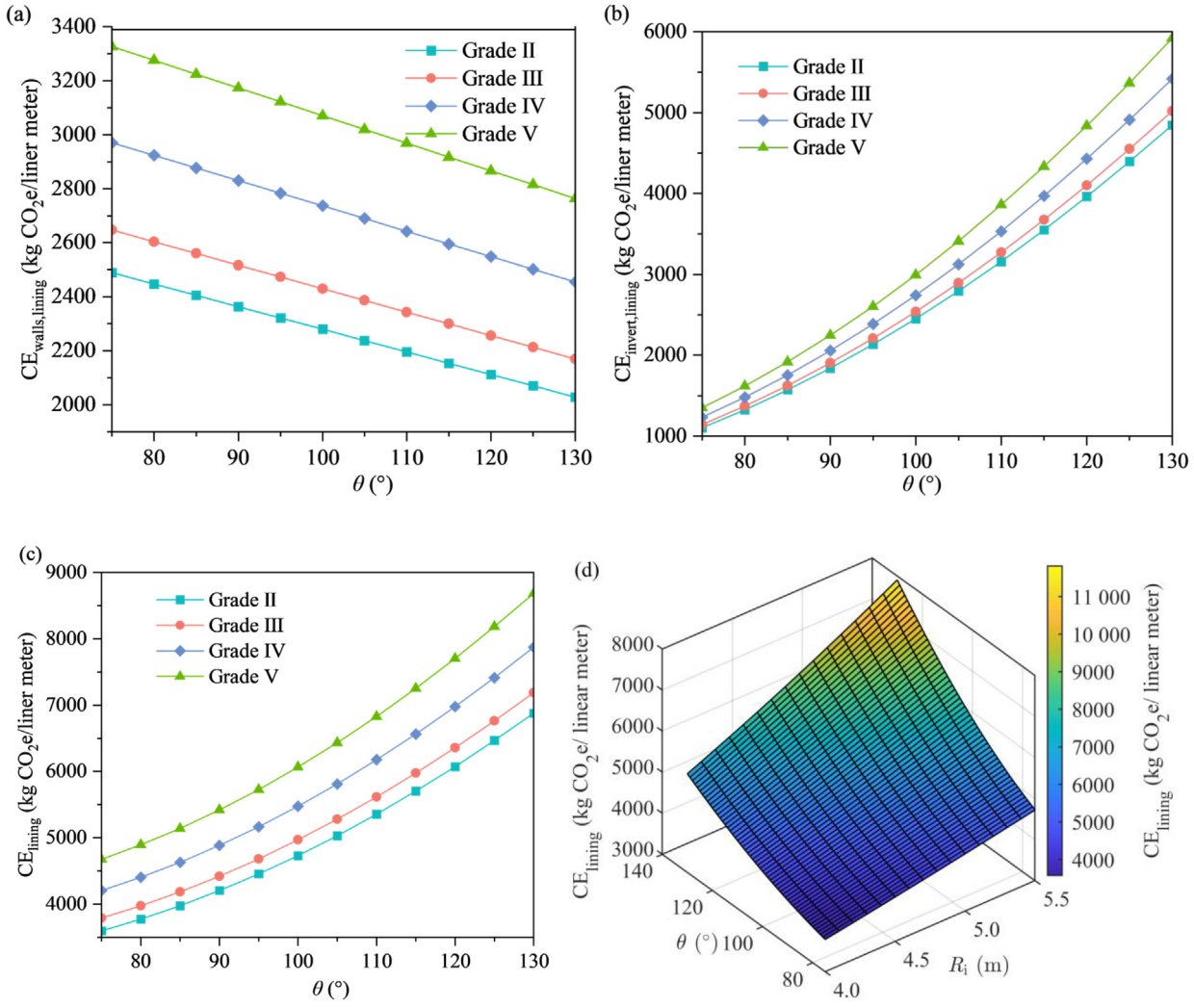

Fig. 15. Effects of design elements on carbon emissions from lining based on (a) θ and arch wall carbon emissions, (b) θ and invert carbon emissions, (c) θ and lining carbon emissions, and (d) θ, R_i, and lining carbon emissions.

tration resistance of the TBM cutter head. This improves the drilling efficiency under constant torque conditions, significantly decreasing the specific energy consumption and associated carbon emissions. In contrast, in hard rock sections, increased penetration resistance leads to accelerated tool wear and shorter replacement cycles, resulting in

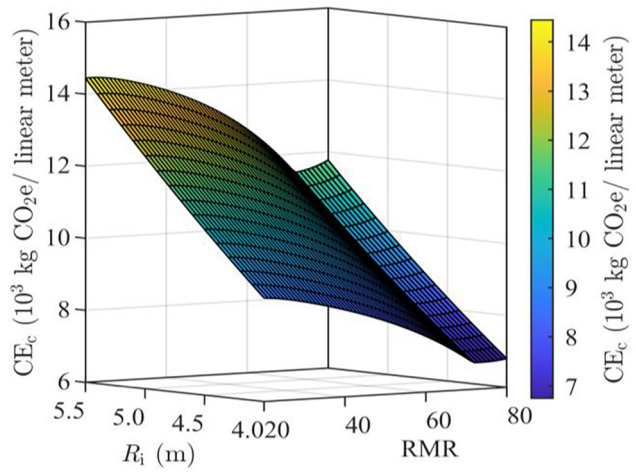

Fig. 16. Effects of design elements on carbon emissions from tunnel construction.

higher maintenance energy consumption and carbon emissions.

The rock mass quality exerts a dual constraint on carbon emissions by influencing the tunneling speed, as illustrated in Fig. 12(b). Within these constraints, the carbon emissions ranged from 2529 to 2950 kg CO_2e/linear meter. Specifically, under Class II rock conditions, the ARA is not minimized, yet carbon emissions reach their peak. In contrast, Class V rock results in the lowest emissions, although an excessively low ARA can negatively affect project scheduling. Class III rocks exhibited a more balanced relationship between ARA and carbon emissions. These findings indicate that maintaining an ARA within the optimal range of 10 to 12 m/d achieves the best balance between energy consumption and carbon emission intensity. Although the theoretical ARA increased in soft rock, the support speed decreased. This interdependency necessitates dynamic coordination during construction to optimize efficiency. Emission reduction can be achieved by coordinating the geology, support, and tunneling parameters. In soft rock sections, adopting a "high-frequency drilling with rapid support" model enhances tunneling efficiency while ensuring timely support. Conversely, in hard rock zones, a "low-frequency impact with delayed support" strategy helps minimize tool wear and maintenance energy consumption, lowering ineffective energy usage.

7.1.2 Effect of LDEs on the carbon emissions of tunnel slag transport

Figure 13 demonstrates that the carbon emissions from tunnel slag transportation exhibited a coupled "geology–transport–energy consumption" relationship. As shown in Fig. 13(a), as the RMR increases, the carbon emissions from slag transportation initially increase and then decrease, fluctuating between 200 and 1000 kg CO_2e/linear meter. Under specific slope conditions, the Class III surrounding rock exhibited the lowest slag transportation emissions. Although lower rocks exhibit reduced density, the fine-grained muck characteristic of Class IV–V rocks (particles >5 mm accounting for <30%) significantly reduces conveyor efficiency, increasing carbon emissions by 15%–20% rather than reducing them. In contrast, Class III rock produces an optimal muck gradation (particles between 5 and 20 mm accounting for >45%), achieving peak transport energy efficiency with emissions as low as 400 kg CO_2e/linear meter. The slope exerts an even greater influence on energy consumption; a 5° increase in the slope results in approximately 30% higher emissions, primarily owing to increased gravitational resistance and accelerated equipment wear. Therefore, employing muck improvement technologies and optimizing transport schemes can reduce emissions from the slag-handling systems.

7.1.3 Effect of LDEs on the carbon emissions of tunnel shotcrete

Carbon emissions from shotcrete were significantly influenced by the RMR (Xu et al., 2019b). As the sur-

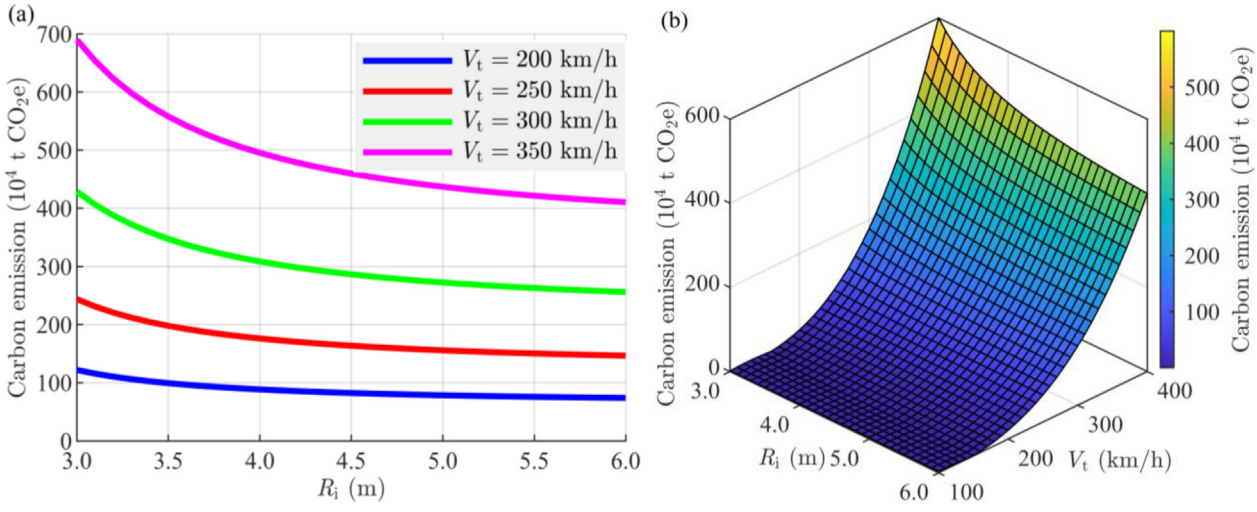

Fig. 17. Effects of R_i and Vt on carbon emissions from a train pulling into tunnel. (a) Static Vt, and (b) dynamic Vt.

rounding rock grade deteriorated from Class II to Class V, the carbon emissions varied from 1000 to 4000 kg CO_2e/-linear meter. This increase is attributed to the progressive loss of the self-supporting capacity of the rock mass, which necessitates a 40%–60% increase in shotcrete thickness to maintain structural reliability. Consequently, carbon emissions increased by 35%–50% (Fig. 14(a)). This sensitivity originates from the degradation of the f_{ck} of low-grade rock. For example, the uniaxial compressive strength of Class V is only 15 MPa, representing a 40% decline compared with Class II, necessitating significantly increased support parameters. In addition, the surrounding rock pressure increases nonlinearly with burial depth. When the depth exceeded 400 m, the rate of pressure increase accelerated, requiring a higher f_{ck} and increasing the carbon emission factor of the material (Fig. 14(b)).

The tunnel excavation radius significantly influences the carbon emissions through both volume and stress mechanisms. For each 1 m increase in radius, the shotcrete volume increases by 25%, directly increasing carbon emissions. Although a larger radius reduces the local stress concentration, it also expands the plastic zone of the surrounding rock, necessitating a higher f_{ck} for structural stability, which further increases carbon emissions. Under Class V surrounding rock conditions, a depth of 500 m, and a radius of 6 m, carbon emissions from the support can reach 8 t CO_2e/linear meter, which is four times higher than the emissions under optimal geological conditions. Nanomodification techniques can be used to enhance the early strength of concrete and shorten the support cycle to mitigate these emissions. In addition, avoiding silty strata and selecting alignments with a rock integrity coefficient >0.5 can help reduce carbon emissions (Zhao et al., 2022). The implementation of a dynamic support system capable of real-time adjustment of shotcrete parameters offers further potential for emission reduction.

7.1.4 Effect of LDEs on the carbon emissions of tunnel lining

The geometric design of the tunnel lining structures, shaped by the base elevation angle and structural curvature, has a significant impact on carbon emissions, as shown in Fig. 15.

As the angle θ increased from 75° to 130°, the carbon emission intensity in the crown area decreased by 17%–20% due to a reduction in support material requirements (Fig. 15(a)). In contrast, emissions in the arch area increased by 18%–28% owing to the increased demand for concrete fill (Fig. 15(b)). As a result, the total emissions from the lining continued to increase because the reduction from the arch walls was insufficient to compensate for the increase from the arch (Fig. 15(c)). In addition, a larger tunnel radius results in a 15%–20% increase in emissions, resulting from a weaker concrete self-balancing effect and greater formwork losses (Fig. 15(d)). Engineering practices can adopt variable cross-sectional designs to minimize emissions at the crown while controlling the rise from the arch to manage carbon emissions. In large-radius segments, the combination of prestressed anchors with lightweight concrete systems can further reduce emissions.

Figure 16 illustrates the impact of the tunnel radius and surrounding rock grades on the carbon emission of the tunnel construction. Rock mass quality and excavation radius served as key driving factors, causing carbon emissions to fluctuate between 7 and 15 t per linear meter, which aligns with the findings reported by Rodríguez and Pérez (2020). A decrease in rock mass quality results in an exponential increase in the support strength requirements. For example, carbon emissions in Class II surrounding rock segments reach 8.5 t per linear meter, whereas in Class V segments, they escalate to 12.3 t per linear meter, representing a 44% increase. In addition, an increase in the excavation radius produces a surface area expansion effect, increasing carbon emissions by approximately 12%–18% for each additional meter. In a segment with a 6 m radius, carbon emissions reach 13 t per linear meter, marking a 22% increase compared to the 5 m segment. The support structure contributes to approximately 70% of the total carbon emissions, with the strength requirements being inversely related to the rock mass quality and directly related to the excavation radius. This illustrates the cumulative effect of decreasing the rock mass grade and increasing the radius on carbon emissions. Designs should align support measures with rock quality by utilizing advanced grouting and fiberglass anchor rods in Class IV–V segments to mitigate carbon emissions. In addition, dynamic radius optimization supported by building information modeling (BIM) analysis can refine the cross-sectional shape and reduce the equivalent radius, further lowering emissions.

In addition, the ARA of the TBM is associated with energy consumption, ventilation, and water treatment (Rodríguez & Pérez, 2020), although its relative contribution to the overall emissions remains limited. These findings have practical value for planning. The implementation of intelligent TBM control and dynamic adjustment of the cutterhead speed and thrust can optimize excavation rates, decrease energy consumption, improve muck removal efficiency, and ultimately reduce carbon emissions.

7.2 Influence of LDEs on carbon emissions of tunnel operation

Figure 17 shows the pattern of carbon emissions resulting from train traction energy consumption during railway tunnel operation, which ranges from 1 to 7 million tons. This variability arises from the dynamic coupling effects between the tunnel cross-sectional dimensions and train operating speed. Higher train speeds increase air resistance, increase traction energy consumption, and correspondingly increase carbon emissions. In addition, the piston effect generated by high-speed trains with speeds of 350 km/h alters the temperature field of the tunnel, causing short-term temperature fluctuations. An increase in the tunnel radius enhances the heat dissipation, reduces the tempera-

ture gradient, and consequently decreases the energy demand of the auxiliary system of the train. The model indicates that each 1 m increase in tunnel radius raises construction-related carbon emissions by 30%–45% but lowers operational emissions by 35%–50%, highlighting a critical trade-off between construction and operational impacts.

To address future low-carbon requirements for transportation infrastructure, it is essential to develop a multi-parameter collaborative optimization theory for tunnel design. The optimal tunnel radius that minimizes the lifecycle carbon emissions under specific geological conditions was identified by constructing detailed numerical models. In addition, a speed-radius collaborative optimization strategy and a multi-objective optimization model can be formulated based on the response surface methodology to determine the optimal matching patterns between various speed ranges and tunnel geometries. This approach aids in reducing carbon emissions and provides a systematic forward-looking theoretical guidance for low-carbon tunnel design.

8 Conclusions

8.1 Conclusions and recommendations

This study addresses key scientific issues in low-carbon design for railway tunnel engineering by innovatively developing a multi-layer integrated framework for the carbon footprint assessment of tunnel projects. It systematically analyzes the pathways through which LDEs influence carbon footprints and, on this basis, examines the nonlinear relationship between LDEs and carbon emissions, demonstrating the significant influence of core elements. This provides a quantifiable, low-carbon decision-making framework for supporting tunnel designs. The findings showed that the TBM shaft, slag transport, shotcrete, and lining primarily drove the carbon footprint during the construction phase. Carbon emissions exhibit significant threshold characteristics in relation to the sensitivity of the excavation radius and the grade of the surrounding rock, thereby providing precise regulatory foundations for optimizing the support design parameters. During the operational phase, the energy consumption is influenced by the interaction between the tunnel radius and train speed, creating a trade-off between increasing the tunnel radius to reduce the traction energy consumption and the associated increase in material usage.

This study focused on tunnel carbon emissions from a design-oriented perspective and provides practical solutions for carbon management throughout the tunnel engineering lifecycle. During the design phase, engineers can utilize the LDE-carbon emission quantitative model to simulate carbon thresholds by inputting variables, such as rock mass quality classification, excavation radius, and support schemes. This assists in optimizing the structural designs. During the construction phase, based on the identified carbon footprint drivers, construction teams can implement a graded management system to improve high-carbon activities, such as TBM tunneling, slag transportation, and material consumption for support and lining. This process management enhances the carbon emission efficiency. During the operational phase, operators can apply the tunnel radius-train speed-energy consumption model to develop dynamic energy-saving strategies, such as adjusting train speed ranges and achieving a balance between energy consumption and carbon emissions. This study introduced a data-driven multi-factor collaborative carbon prediction method that integrates design parameters with construction and operational carbon emissions, overcoming the limitations of traditional empirical decision-making.

8.2 Limitations and future work

Although this study revealed the mechanisms by which the tunnel engineering design affects carbon emissions during construction and operation, thereby providing a theoretical foundation for source-level emission control, several limitations remain that warrant further investigation.

First, this study did not analyze the carbon emissions associated with commonly used construction methods such as shield tunneling and drill-and-blast techniques. Future research should focus on establishing a lifecycle carbon footprint assessment model that includes interactions among multiple construction methods. Such a model would enable dynamic simulation and horizontal comparison of carbon emission intensities of different construction schemes, thereby providing scientific and quantitative decision support for the selection of green construction schemes.

Second, the applicability of these findings to specific geological conditions requires further validation. Under karst geological conditions, processes such as advanced support and cavity grouting increase the cement consumption. The waiting time for grouting and curing decreases the mechanical construction efficiency, indirectly increasing the carbon emission intensity. In permafrost environments, reduced equipment efficiency and increased use of insulation material alter the distribution of carbon emissions. Future studies should develop adaptive algorithms based on geological features and create a carbon emissions prediction platform designed for various geological settings.

Finally, this study simplified the influence of auxiliary materials and construction machinery, leading to systematic errors. Future studies should aim to develop a collaborative platform with nested dynamic carbon measurements and parametric correction modules. Carbon emissions accounting is enhanced by analyzing the nonlinear cumulative effects. A dynamic calibration mechanism for the boundary conditions was also established to mini-

mize errors and create a universal method for accurately predicting carbon emissions in tunnel engineering projects.

Data availability

The data that support the findings of this study are available from the corresponding author upon reasonable request.

CRediT authorship contribution statement

Yajuan Li: Writing – review & editing, Writing – original draft, Visualization, Validation, Supervision, Software, Methodology, Investigation, Formal analysis, Data curation, Conceptualization. **Xueying Bao:** Writing – review & editing, Resources, Project administration, Funding acquisition.

Declaration of competing interest

The authors declare that they have no known competing financial interests or personal relationships that could have appeared to influence the work reported in this paper.

Acknowledgement

This work was supported by the Science and Technology Program of Gansu Province (Grant No. 25YFFA016).

References

Alber, M., Yarali, O., Dahl, F., & Bruland, A. (2014). ISRM suggested method for determining the abrasivity of rock by the CERCHAR abrasivity test. *Journal of Rock Mechanics and Geotechnical Engineering, 47*(1), 261–266.

Alkan, M., İnce, H. H., Çakiroğlu, M. A., & Süzen, A. A. (2021). Prediction of rebound amount in dry mix shotcrete by a fast-adaboosting neural network. *Tehnicki Vjesnik, 28*(2), 426–432.

Aldrian, W., Bantle, A., & Juhart, J. (2022). CO_2 reduction in tunnel construction from a material technology point of view. *Geomechanics and Tunnelling, 15*(6), 799–810.

Bastidas-Arteaga, E., Schoefs, F., Stewart, M. G., & Wang, X. (2013). Influence of global warming on durability of corroding RC structures: A probabilistic approach. *Engineering Structures, 51*, 259–266.

Bai, Y., Mao, B., Zhou, F., Ding, Y., & Dong, C. (2009). Energy-efficient driving strategy for freight trains based on power consumption analysis. *Journal of Transportation Systems Engineering & Information Technology, 9*(3), 43–50.

Chen, X., Huang, M., Bai, Y., & Zhang, Q. (2024). Sustainability of underground infrastructure – Part 1: Digitalisation-based carbon assessment and baseline for TBM tunnelling. *Tunnelling and Underground Space Technology, 148*, 105776.

Chen, X., Huang, M., Xiao, F., Bai, Y., & Zhang, Q. B. (2025). Sustainability of underground infrastructure – Part 2: Digitalisation-based integration and optimisation for low carbon design. *Tunnelling and Underground Space Technology, 159*, 106479.

China Railway (2018). Q/CR 9004—2018: Specification for Construction Organization Design of Railway Engineering. Beijing: China Railway Publishing House (in Chinese).

Climate Change Department of the Ministry of Ecology and Environment of the People's Republic of China (2025). *Announcement on the release of 2023 electricity carbon footprint factor data*. China: Beijing (in Chinese).

Cornet, Y., Dudley, G., & Banister, D. (2018). High speed rail: Implications for carbon emissions and biodiversity. *Case Studies on Transport Policy, 6*(3), 376–390.

Dammyr, Ø., Nilsen, B., Thuro, K., & Grøndal, J. (2014). Possible concepts for waterproofing of Norwegian TBM railway tunnels. *Rock Mechanics and Rock Engineering, 47*, 985–1002.

Denning, A. S. (2018). Combustion to concentration to warming: What do climate targets mean for emissions? climate change and the global carbon cycle. *Encyclopedia of the Anthropocene, 1*, 443–452.

Doulos, L. T., Sioutis, I., Tsangrassoulis, A., Canale, L., & Faidas, K. (2020). Revision of threshold luminance levels in tunnels aiming to minimize energy consumption at no cost: Methodology and case studies. *Energies, 13*(7), 1707.

Fang, J., Luo, B., & Liu, H. (2021). Quantitative analysis and calculation of concrete consumption in railway tunnels. *Tunnel Construction, 41*(5) , 721–728 (in Chinese).

Farrokh, E. (2021). Cutter change time and cutter consumption for rock TBMs. *Tunnelling and Underground Space Technology, 114*, 104000.

Fazeli, H., & Peng, Q. (2022). Generation and evaluation of product concepts by integrating extended axiomatic design, quality function deployment and design structure matrix. *Advanced Engineering Informatics, 54*, 101716.

Golser, J., Friess, J., & Luniaczek, T. (2022). CO_2 reduction in tunnelling from the point of view of construction design and implementation. *Geomechanics and Tunnelling, 15*(6), 792–798.

Guo, Y., Sun, W., Xu, H., He, W., Chen, Z., & Guo, C. (2023). Comparison between shield method and drill and blast method regarding carbon emission intensity in subway tunnel construction. *Modern Tunnelling Technology, 60*(3), 14–23+64 (in Chinese).

Guo, C., Wang, M., Lu, Y., Zhitao, S., Yunlong, Z., & Xu, J. (2016). A review of energy consumption and saving in extra-long tunnel operation ventilation in China. *Renewable and Sustainable Energy Reviews, 53*, 1558–1569.

Guo, Y., Chen, D., Chen, Z., Zhao, S., Sun, W., He, W., Zhang, L., Wang, Y., Hu, N., & Guo, C. (2025a). Evaluation of greenhouse gas emissions in subway tunnel construction. *Underground Space, 22*, 263–279.

Guo, G., Li, X., Zhu, C., Wu, Y., Chen, J., Chen, P., & Cheng, X. (2025b). Establishing benchmarks to determine the embodied carbon performance of high-speed rail systems. *Renewable and Sustainable Energy Reviews, 207*, 114924.

He, B., Wang, W., Zhu, X., & Qian, S. (2023). Integrate design structure matrix with carbon footprint for product low carbon design. *Advanced Engineering Informatics, 56*, 102021.

Hopf, B. W., Hoxha, E., Scherz, M., Heichinger, H., Kreiner, H., & Passer, A. (2022). Life cycle assessment of tunnel structures: Assessment of the New Austrian tunnelling method using a case study. *IOP Conference Series: Earth and Environmental Science, 1078*(1), 012117.

Huang, L., Jakobsen, P. D., Bohne, R. A., Liu, Y., Bruland, A., & Manquehual, C. J. (2020). The environmental impact of rock support for road tunnels: The experience of Norway. *Science of the Total Environment, 712*, 136421.

IStructE. (2022). How to calculate embodied carbon, IStructE Guide. *The Institution of Structural Engineers*, London, United Kingdom.

Jian, L., Qiu, W., & Cheng, Y. (2024). Accurate estimation of concrete consumption in tunnel lining using terrestrial laser scanning. *Scientific Reports, 14*(1), 2705.

Jun, P., Li, W., Yan, L., Yuan, X., & Zi, X. (2019). Innovative product design method for low-carbon footprint based on multi-layer carbon footprint information. *Journal of Cleaner Production, 228*, 729–745.

Kanyilmaz, A., Hoidang, V., & Kondratenko, A. (2023). How does conceptual design impact the cost and carbon footprint of structures? *Structures, 58*, 105102.

Kim, K. Y., Jo, S. A., Ryu, H. H., & Cho, G. C. (2020). Prediction of TBM performance based on specific energy mechanical properties and failure mechanisms of sandstone with pyrite concretions under uniaxial compression. *Geomechanics and Engineering, 21*(6), 489–496.

Kong, L., Wang, L., Li, F., Lv, X., Li, J., Ma, Y., Chen, B., & Guo, J. (2021). Multi-layer integration framework for low carbon design based on design features. *Journal of Manufacturing Systems, 61*, 223–238.

Lee, J. Y., & Ellingwood, B. R. (2017). A decision model for intergenerational life-cycle risk assessment of civil infrastructure exposed to hurricanes under climate change. *Reliability Engineering & System Safety, 159*, 100–107.

Li, P., Liu, H., Zhao, Y., & Li, Z. (2018). A bottom-to-up drainage and water pressure reduction system for railway tunnels. *Tunnelling and Underground Space Technology, 81*, 296–305.
Liu, Q. S., Liu, J. P., & Pan, Y. C. (2016). Research advances of tunnel boring machine performance prediction models for hard rock. *Chinese Journal of Rock Mechanics and Engineering, 35*(S1), 2766–2786 (in Chinese).
Liu, T., Zhu, H., Shen, Y., Li, T., & Liu, A. (2024). Embodied carbon assessment on road tunnels using integrated digital model: Methodology and case-study insights. *Tunnelling and Underground Space Technology, 143*, 105485.
Ma, J., He, S., Liu, X., & He, J. (2023). Research and optimization of tunnel construction scheme for super-large span high-speed railway tunnel in poor tuff strata. *Applied Rheology, 33*(1), 20230101.
Ma, S., Yan, H., Li, D., Liu, H., & Zeng, H. (2025). The impact of agricultural mechanisation on agriculture carbon emission intensity: Evidence from China. *Pakistan Journal of Agricultural Sciences, 62*(1), 99–110.
Ministry of Housing and Urban-Rural Development of the People's Republic of China (2019). *GB/T 51366—2019: Standard for building carbon emission calculation*. Beijing, China: China Building Industry Press (in Chinese).
National Railway Administration of the People's Republic of China (NRA). (2016). *TB 10003—2016: Code for design of railway tunnel*. Beijing, China: China Railway Publishing House. (in Chinese).
NRA. (2017). *TZJ 2003—2017: Budget quota of railway engineering (Volume 3): Tunnel engineering*. Beijing, China: China Railway Publishing House (in Chinese).
NRA. (2018). *TB/T 1407.1—2018: Railway train traction calculation Part 1: Trains with locomotives*. China Railway Publishing House, Beijing, China (in Chinese).
NRA. (2024). *TB 10068—2024: Code for design on operating ventilation of railway tunnel*. Beijing, China: China Railway Publishing House (in Chinese).
Peng, J., Li, W., Li, Y., Xie, Y., & Xu, Z. (2019). Innovative product design method for low-carbon footprint based on multi-layer carbon footprint information. *Journal of Cleaner Production, 228*, 729e745.
Pritchard, J. A., & Preston, J. (2018). Understanding the contribution of tunnels to the overall energy consumption of and carbon emissions from a railway. *Transportation Research Part D: Transport and Environment, 65*, 551–563.
Richard, Z. T., & Celada, B. (2012). Specific energy of excavation in detecting tunnelling conditions ahead of TBMs. *Tunnels & Tunnelling International, 2012*(Feb.), 65–68.
Rodríguez, R., Bascompta, M., & García, H. (2024). Carbon footprint evaluation in tunnels excavated in rock using tunnel boring machine (TBM). *International Journal of Civil Engineering, 22*(6), 995–1009.
Rodríguez, R., & Pérez, F. A. (2020). Carbon foot print evaluation in tunneling construction using conventional methods. *Tunnelling and Underground Space Technology, 108*, 103704.
She, L., Zhang, S., Wang, C., Li, Y., & Du, M. (2023). A new method for wear estimation of TBM disc cutter based on energy analysis. *Tunnelling and Underground Space Technology, 131*, 104840.
Shi, X., Kou, L. M., Liang, H., Wang, Y., & Li, W. (2024). Evaluating carbon emissions during slurry shield tunneling for sustainable management utilizing a hybrid life-cycle assessment approach. *Sustainability, 16*(7), 2702.
Song, Y., Zhu, H., Shen, Y., Yan, Z., & Feng, S. (2024a). Zero-carbon tunnels: Concepts, methodology, and applications in the built environment. *Journal of Cleaner Production, 479*, 144031.
Song, Y., Zhu, H., Shen, Y., & Feng, S. (2024b). Green tunnel lighting environment: A systematic review on energy saving, visual comfort and low carbon. *Tunnelling and Underground Space Technology, 144*, 105535.
Spyridis, P., & Bergmeister, K. (2024). Sustainable tunnel design: Concepts and examples of reducing greenhouse gas emissions through basic engineering assumptions. *Tunnelling and Underground Space Technology, 152*, 105886.
Sun, H. M., & Park, Y. (2020). CO_2 emission calculation method during construction process for developing BIM-based performance evaluation system. *Applied Energy, 10*(16), 5587.
Tien, N. T., Anh, D. H., Anatolyevich, K. M., Kien, D. V., & Daniel, D. (2020). Tunnel shape influence on the tunnel lining behavior. *Geotechnical Engineering, 174*(4), 355–371.
Wang, J., Hou, X., Deng, X., Han, H., & Zhang, L. (2022). Application of BIM in tunnel design with compaction pile reinforced foundation carrying carbon assessment based on advanced dynamo visual programming: A case study in China. *Sustainability, 14*(23), 16222.
Wang, Y., Du, P., Chen, Y., Hua, S., Wang, J., Shi, C., & Liu, K. (2023). Mixed ventilation approach combined with single-shaft complementary system for highway tunnels. *Tunnelling and Underground Space Technology, 132*, 104927.
Wang, Z., Wang, F., & Ma, S. (2025). Research on the coupled and coordinated relationship between ecological environment and economic development in China and its evolution in time and space. *Polish Journal of Environmental Studies, 34*(3), 3333–3342.
Wang, Z., & Ma, S. (2024). Research on the impact of digital inclusive finance development on carbon emissions—Based on the double fixed effects model. *Global NEST Journal, 26*(7), 06227.
Wu, Y., Wu, H., Gong, C., & Huang, L. (2023). Numerical investigation of key structural parameters for middle-buried rubber waterstops. *Mathematics, 11*(16), 3546.
Xu, J. F., Guo, C., Chen, X. F., Zhang, Z. H., Lu, Y., Wang, M. N., & Yang, K. (2019a). Emission transition of greenhouse gases with the surrounding rock weakened – A case study of tunnel construction. *Journal of Cleaner Production, 209*, 169–179.
Xu, J. F., Guo, C., & Yu, L. (2019b). Factors influencing and methods of predicting greenhouse gas emissions from highway tunnel construction in Southwestern China. *Journal of Cleaner Production, 229*(20), 337–349.
Xu, J. F., Dong, C., Guo, D., & Guo, C. (2021). Influence of lining design parameters on the greenhouse gas emissions of Chinese highway tunnel construction. *Transportation Research Record, 2675*(11), 685–698.
Xu, J. F., Xu, Z. L., Guo, C., Yuan, K., Dong, H. J., Yang, X. B., Yang, Y. P., Tian, Y., & Chen, Y. Q. (2023). Characteristics of carbon emissions from excavation and supporting during construction of inclined shafts of highway tunnels. *Tunnel Construction, 43*(7), 1146–1152 (in Chinese).
Xue, Y., Zhao, F., Zhao, H., Li, X., & Diao, Z. (2018). A new method for selecting hard rock TBM tunnelling parameters using optimum energy: A case study. *Tunnelling and Underground Space Technology, 78*, 64–75.
Yi, C., Gwak, H., & Lee, D. (2016). Stochastic carbon emission estimation method for construction operation. *Journal of Civil Engineering and Management, 23*(1), 137–149.
Yin, X., Zhang, Y., Zhong, K., & Bian, W. (2023). Research on anchorage parameters and support design of prestressed anchors in shallow buried large span tunnels. *Metal Mine, 2*, 58–66 (in Chinese).
Zhang, Z., Zhang, H., & Tan, Y. (2018). Natural wind utilization in the vertical shaft of a super-long highway tunnel and its energy saving effect. *Building and Environment, 145*, 140–152.
Zhao, J., Feng, Y., & Yang, C. (2021). Intelligent control and energy saving evaluation of highway tunnel lighting: Based on three-dimensional simulation and long short-term memory optimization algorithm. *Tunnelling and Underground Space Technology, 109*, 103768.
Zhao, J., Kou, L., Jiang, Z., Lu, N., Wang, B., & Li, Q. (2022). A novel evaluation model for carbon dioxide emission in the slurry shield tunnelling. *Tunnelling and Underground Space Technology, 13*, 104757.
Zhou, Y., Yang, Y., Bu, R., Ma, F., & Shen, Y. (2020). Effect of press-in ventilation technology on pollutant transport in a railway tunnel under construction. *Journal of Cleaner Production, 243*, 118590.